Coherent structures and turbulence evolution in magnetized non-neutral plasmas

M. Romé[1,2], S. Chen[3], G. Maero[1,2] and R. Pozzoli[1,2]

[1] Department of Physics, University of Milano, Italy
[2] INFN, Sec. of Milano, Italy
[3] Institute of Fluid Physics, China Academy of Engineering Physics, Mianyang, China

Outline

- Non-neutral plasmas and 2D ideal fluid isomorphism

- 2D electron plasma turbulence: numerical simulations and wavelet analysis
  - Free relaxation
  - Forced dynamics

- Conclusions and perspectives

# Non-neutral plasmas and 2D ideal fluid isomorphism

Penning–Malmberg Trap

Magnetized non-neutral plasmas can be easily confined for long times in Penning-Malmberg traps under UHV conditions (p < 10^{-8} mbar) with a combination of static electric and magnetic fields, and their evolution can be monitored by means of electrostatic and optical systems.
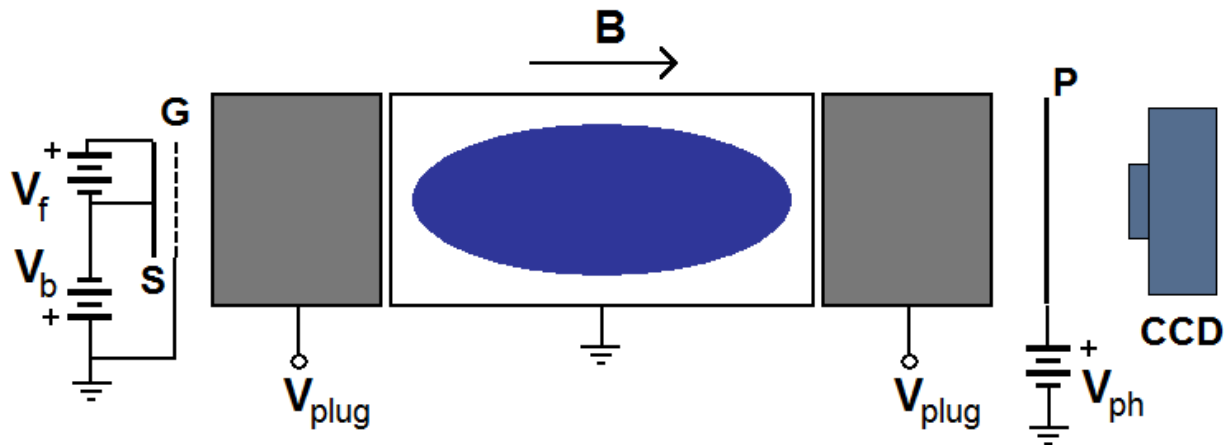
(Typical) PM trap operation:
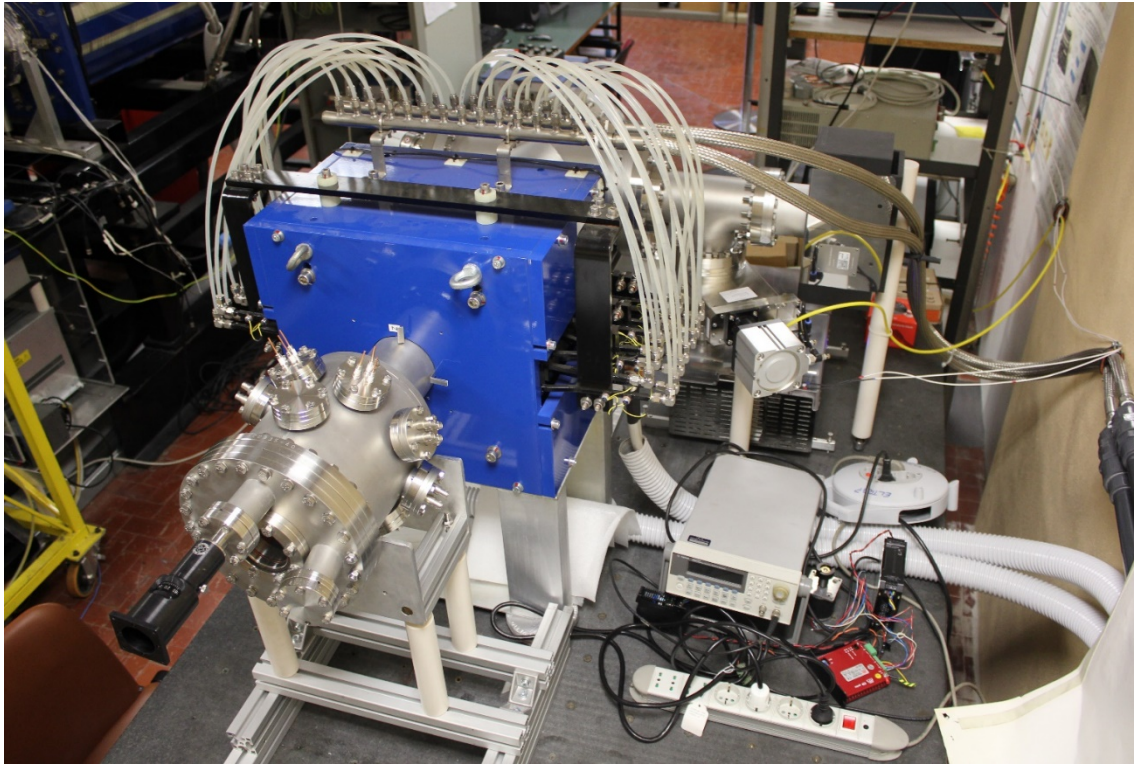generate (inject) / hold&manipulate /dump&measure

ELTRAP device @ Milano University
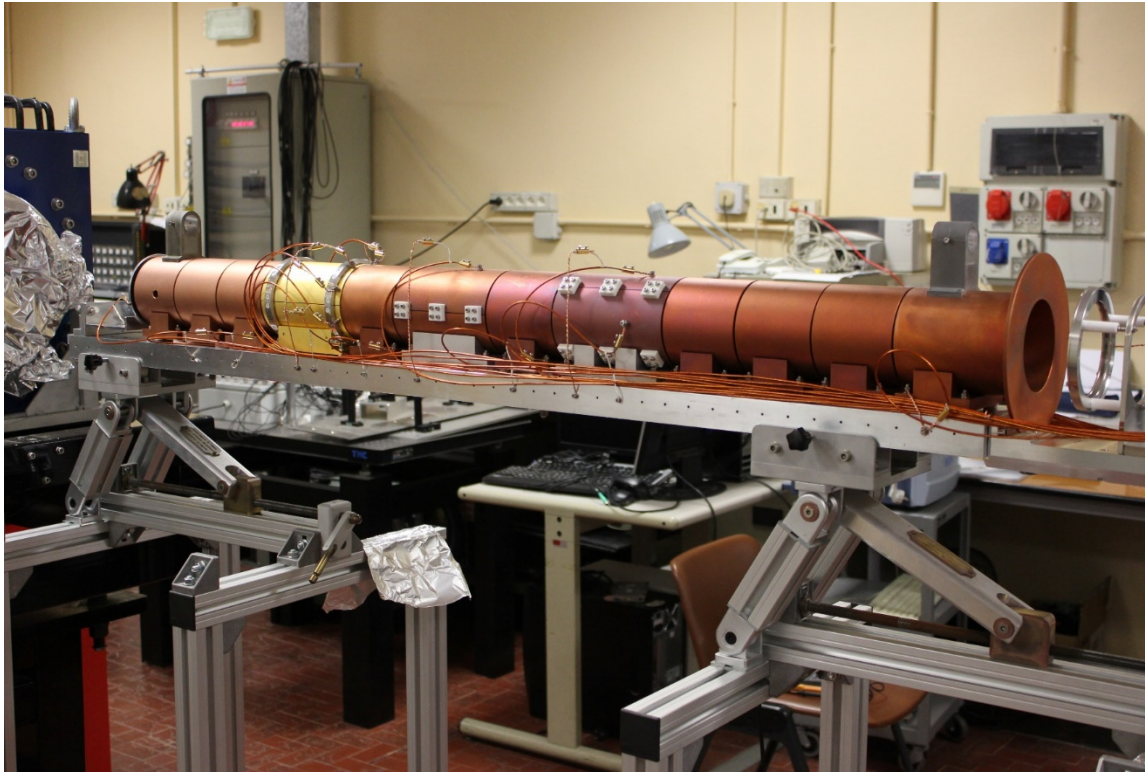
Parameter	Range
n_e	$10^6 - 10^8$ cm^{-3}
B	≤ 0.2 T
T_e	1 - 10 eV
p	$10^{-9} - 10^{-8}$ mbar
$|V_{plug}|$	≤ 100 V
L_p	10 - 100 cm
R_w	4.5 cm

Amoretti et al, RSI 2003; Maero et al, JPP 2015

DuEl device @ Milano University

Parameter	Range
n_e	$10^6 - 10^8$ cm^{-3}
B	$\leq$ 0.88 T
T_e	1 - 10 eV
p	$10^{-9} - 10^{-8}$ mbar
$|V_{plug}|$	$\leq$ 200 V
L_p	5 – 25 cm
R_w	2.25 cm

Romé et al, AIP Proc. 1668 (2015)

2D ideal fluid isomorphism

$$(2\pi\varepsilon_0 B / en)(T / m)^{1/2} / L \gg 1$$

- Guiding center electrostatic approximation;
- averaging over the bounce motion;
- perpendicular dynamics determined by the ExB-drift only.

2D Ideal Fluid	2D Electron Plasma
$\frac{\partial \zeta}{\partial t} + \mathbf{v} \cdot \nabla \zeta = 0$	$\frac{\partial n}{\partial t} + \mathbf{v} \cdot \nabla n = 0$
$\nabla^2 \psi = \zeta$	$\nabla^2 \phi = 4\pi en$
$\mathbf{v} = \mathbf{e}_z \times \nabla \psi$	$\mathbf{v} = \frac{\mathbf{e}_z \times \nabla \phi}{B} c$
$\zeta = (\nabla \times \mathbf{v}) \cdot \mathbf{e}_z$	$\zeta = \frac{c}{B} \nabla^2 \phi = \frac{4\pi ec}{B} n$
$\psi(\text{wall}) = \text{constant}$	$\phi(\text{wall}) = \text{constant}$

Note: the vorticity has a single sign for an electron plasma.

Basic 2D fluid phenomena

Electron plasmas allow to perform experiments on 2D fluid dynamics under almost ideal conditions.

[Non-idealities are introduced by inhomogeneities of the confining fields, finite resistivity of the wall, collisions with neutrals, etc.]
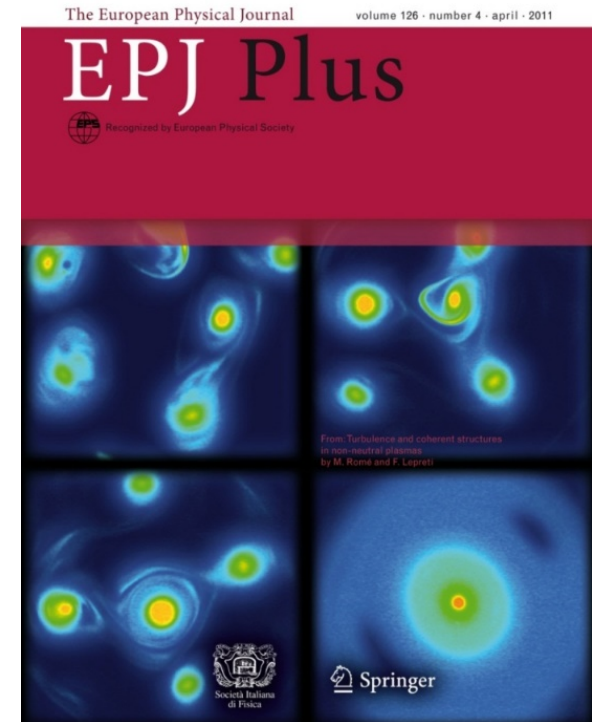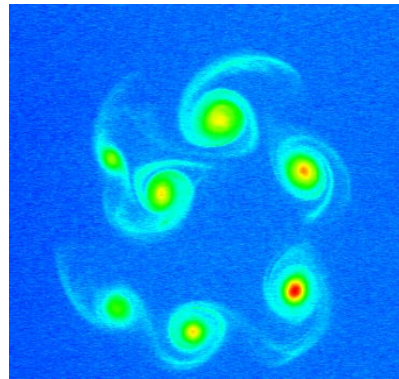

Romé et al, EPJ Plus 2011
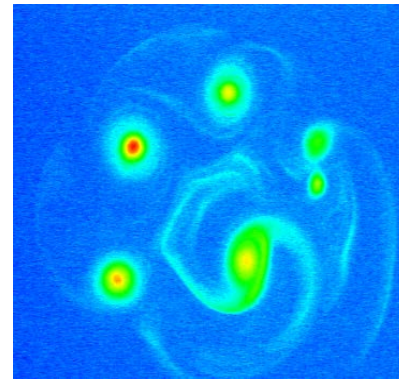
2D fluid dynamics with non-neutral plasmas

The evolution of the system can be reconstructed repeating several inject/hold/dump cycles with an increasing trapping time and with the same initial conditions (injection parameters) [high shot to shot reproducibility].
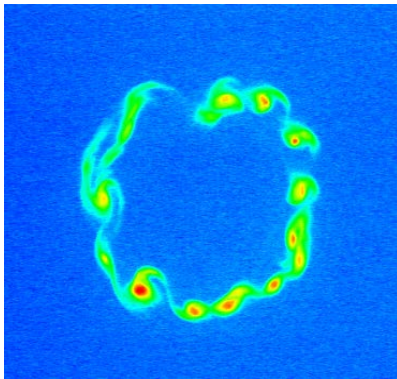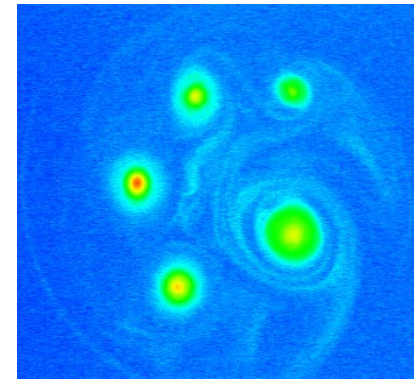

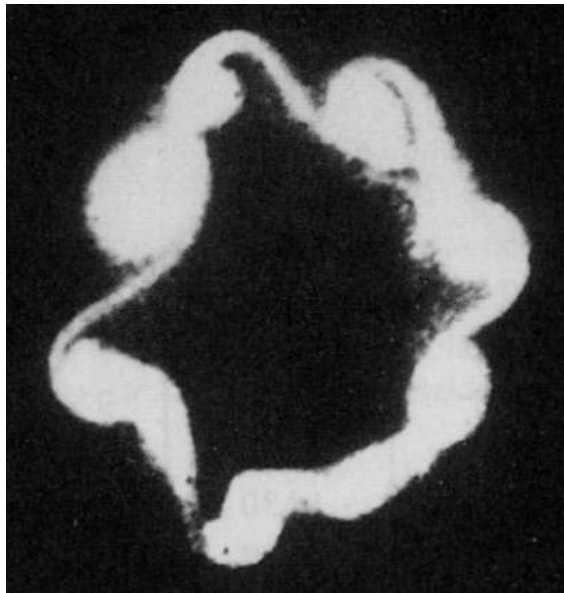| t = 0 μs | t = 20 μs | t = 60 μs | t = 140 μs |

Diocotron (KH) instability

The evolution of the system is dominated by the <u>diocotron (Kelvin-Helmholtz) instability</u> due to the shear of the angular velocity, driving the plasma into a strongly non-linear regime in which vortex structures appear (eventually dissipated by viscosity effects on collisional time scales).

Diocotron vortices
in an electron beam
[Webster, JAP 1955]
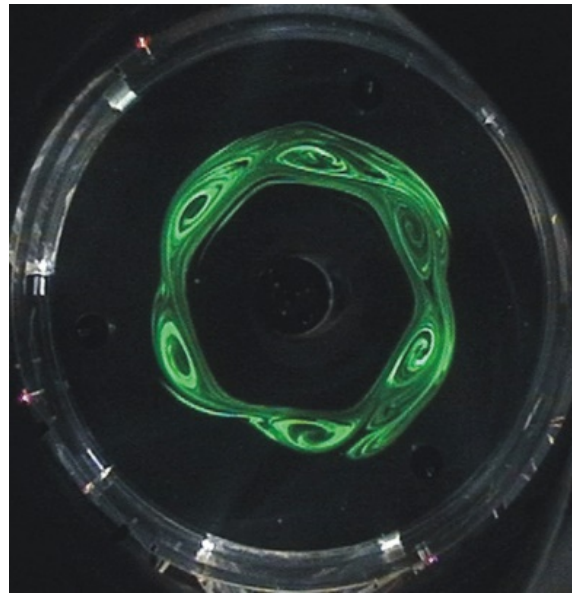
KH-instability of a fluid
in a rotating tank
[Aguiar *et al.*, Icarus 2009]
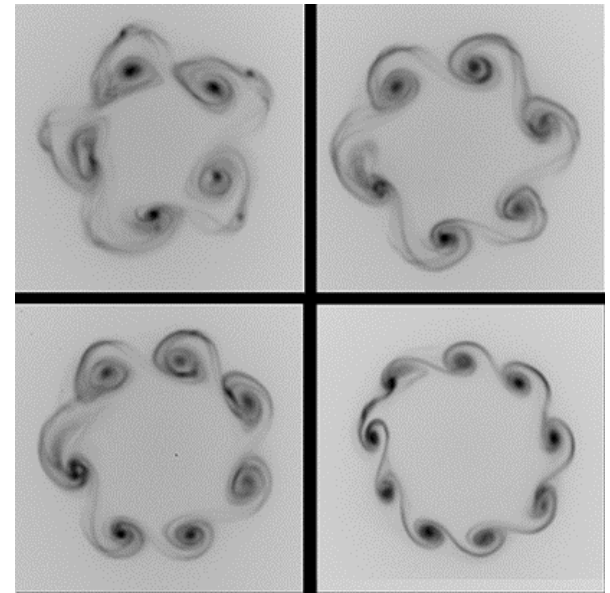
Electron injection into a
Penning-Malmberg trap
[Bettega et al., PoP 2007]

Vortex crystals

The evolution of the system leads sometimes to the formation of stable, rotating vortex patterns ("vortex crystals" [Fine *et al.*, PRL 1995]).

Romé et al, EPJ Plus 2011

2D electron plasma turbulence: numerical simulations and wavelet analysis

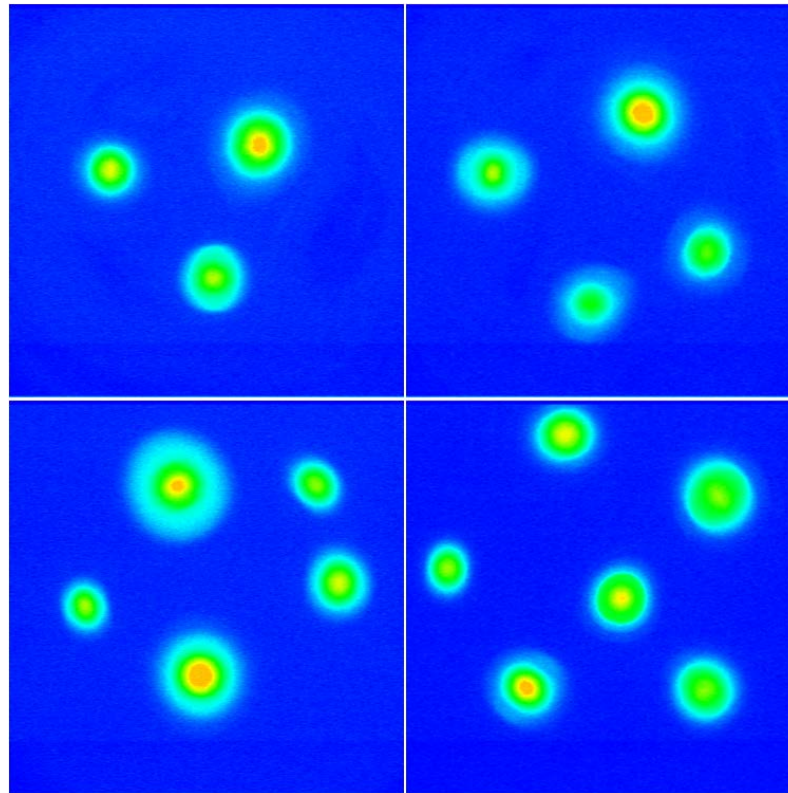# Investigation of the 2D turbulence: literature

The formation and evolution of coherent structures, as well as the manipulation and control of the trapped sample, have been subject of investigation for decades in the non-neutral plasmas community.

The 2D turbulence in pure electron plasmas has been studied by:
- variational principles [Huang et al, PRL 1994; Jin et al, PRL 1998; Rodgers et al, PRL 2009];
- time scaling of the vortices present in the flow [Jin et al, PRL 2000];
- statistical techniques.

E.g., in the so-called punctuated scaling theory [Carnevale et al, PRL 1991] the turbulent flow is assumed to be dominated by the presence of strong coherent structures with the occasional mergers of like-signed vortices. In the so-called 'regional' maximum fluid entropy theory [Jin et al, PRL 1998, PRL 2000], strong vortices in the flow ergodically mix the background, which in turn cools the chaotic motion of the strong vortices, driving them into an equilibrium pattern.

The statistical theories rely on the presence of global constraints, and usually neglect the details of the early dynamical evolution of the flow.

Investigation of the 2D turbulence: motivation

The initial vortex distribution may affect the time evolution of the freely decaying or forced 2D turbulence, since the vortex interactions strongly depend on vortex size, vorticity amplitude, separation of the vortex centers, and background shear induced by the surrounding vortices.

The attempt is to characterize, by means a systematic variation of the initial conditions and of the characteristics of forcing, the parameters playing a major role in the early dynamics of the flow leading to an evolution dominated either by the presence of coherent structures (possibly leading to the formation of vortex crystal-like states), or by a higher turbulence level, and to determine trends or indices that can help in the identification and quantitative characterization of turbulence features.

The analysis is performed with the use of advanced statistical techniques:
- ✓ <u>POD analysis</u> [Romé et al, EPJ Plus 2011];
- ✓ <u>Structure functions</u> [Lepreti et al, PRE 2013; Romé et al, PSST 2016];
- ✓ <u>Wavelet analysis</u> [Kawai et al, PRE 2008; Bettega et al, NJP 2009; Chen et al, JPP 2015; Romé et al, PSST 2016, PPCF 2017; Chen et al, JPP 2017].

2D (transverse plane) modeling [electrons]

$$\frac{\partial n_e}{\partial t} + \left[\phi, n_e\right] = 0, \quad \nabla^2 \phi = n_e,$$

$$\left[\phi, n_e\right] = \frac{1}{r}\left(\frac{\partial \phi}{\partial r}\frac{\partial n_e}{\partial \theta} - \frac{\partial \phi}{\partial \theta}\frac{\partial n_e}{\partial r}\right).$$

$$n_e / n_0, \quad r / R_w, \quad \phi / (en_0 R_w^2 / \varepsilon_0),$$

$$t / (\omega_c / \omega_p^2) = t / (\varepsilon_0 B / en_0);$$

$$\omega_c = eB / m_e, \quad \omega_p = (e^2 n_0 / \varepsilon_0 m)^{1/2}.$$

$$H \equiv -\frac{1}{2}\int r\,dr\,d\theta\, n_e(r,\theta,t)\,\phi(r,\theta,t) = const,$$

$$L \equiv -\frac{1}{2}\int r\,dr\,d\theta\, r^2\, n_e(r,\theta,t) = const,$$

$$Z_j \equiv \frac{1}{j}\int r\,dr\,d\theta\, n_e^{\,j}(r,\theta,t) = const \quad (j \geq 1).$$

2D PIC simulations [1]

A 2D 'hybrid' PIC code has been developed [Maero *et al., EPJD 2014*] in order to investigate the transverse dynamics of an electron(fluid)-ion(kinetic) system:

- Discretization on a Cartesian grid;

- Poisson eq.: double FFT + capacity matrix method; static and/or time-dependent Dirichlet conditions (circular boundary);

- Time advancement: RK4 scheme for electrons, modified VV scheme [Spreiter & Walter, JCP 1999] for the kinetic populations.

2D PIC simulations [2]

Here <u>only the electron population</u> is considered.

Initial density distributions:

- <u>annular</u> (the outer radius r+ of the annulus is varied);
- <u>spiral</u> (the number of turns of the spiral is varied)

The initial area covered by the plasma is the same in all simulations.

$n_0 = 10^7$ cm^{-3};
$B = 1$ T;
$R_w = 2$ cm;
$t_f = 2\text{-}4$ ms;
$dt = 10^{-7}$ s;
$N_{macro} = 1\text{-}2.5 \cdot 10^6$;
$N_{grid} \times N_{grid}$ mesh, with $N_{grid} = 256$ or 512.

Coarse-graining

Experimentally, H and L are *robust* invariants, while Z_j ($j \geq 2$) are *fragile* or *dissipated* invariants [Driscoll et al, PhysA 1999].

H and L are conserved in the PIC simulations with a relative accuracy of the order of 10^{-6}. The PIC method introduces an intrinsic effective "coarse-graining", which causes a non conservation of the topological invariants (with the obvious exception of Z_1) [Schecter et al, PoF 1999; Rodgers et al, PRL 2010].

The density (vorticity) filaments become longer and longer so that their thickness becomes smaller than the experimental resolution (e.g. the pixel size of the optical diagnostics of the density) or smaller than the cell size of the numerical mesh used for the discretization of the 2D Euler equations.
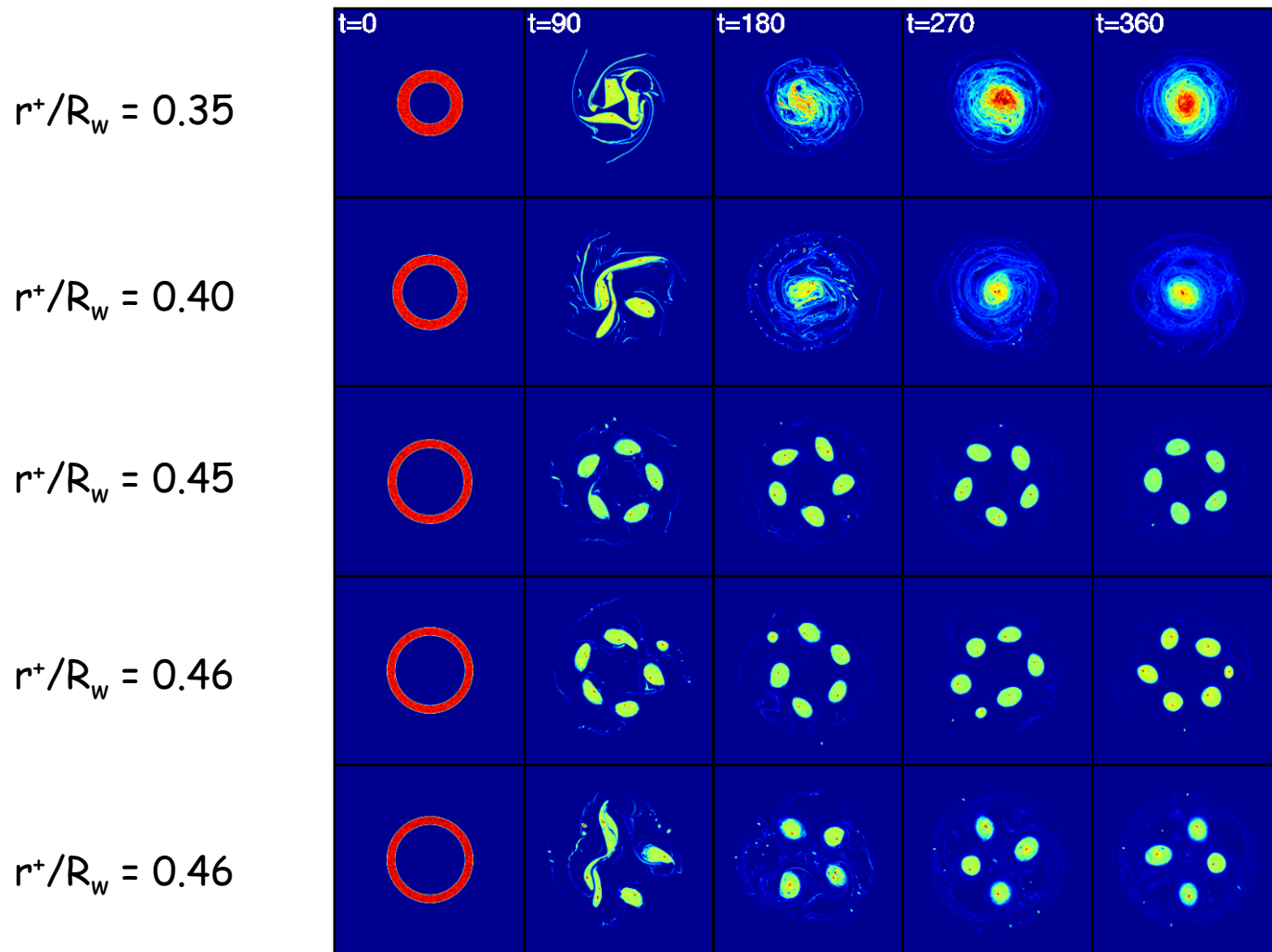
Free relaxation

Influence of initial conditions

The role and evolution of coherent structures in electron plasmas have been studied considering different types of initial conditions: <u>annular</u> and <u>spiral</u> vorticity distributions.
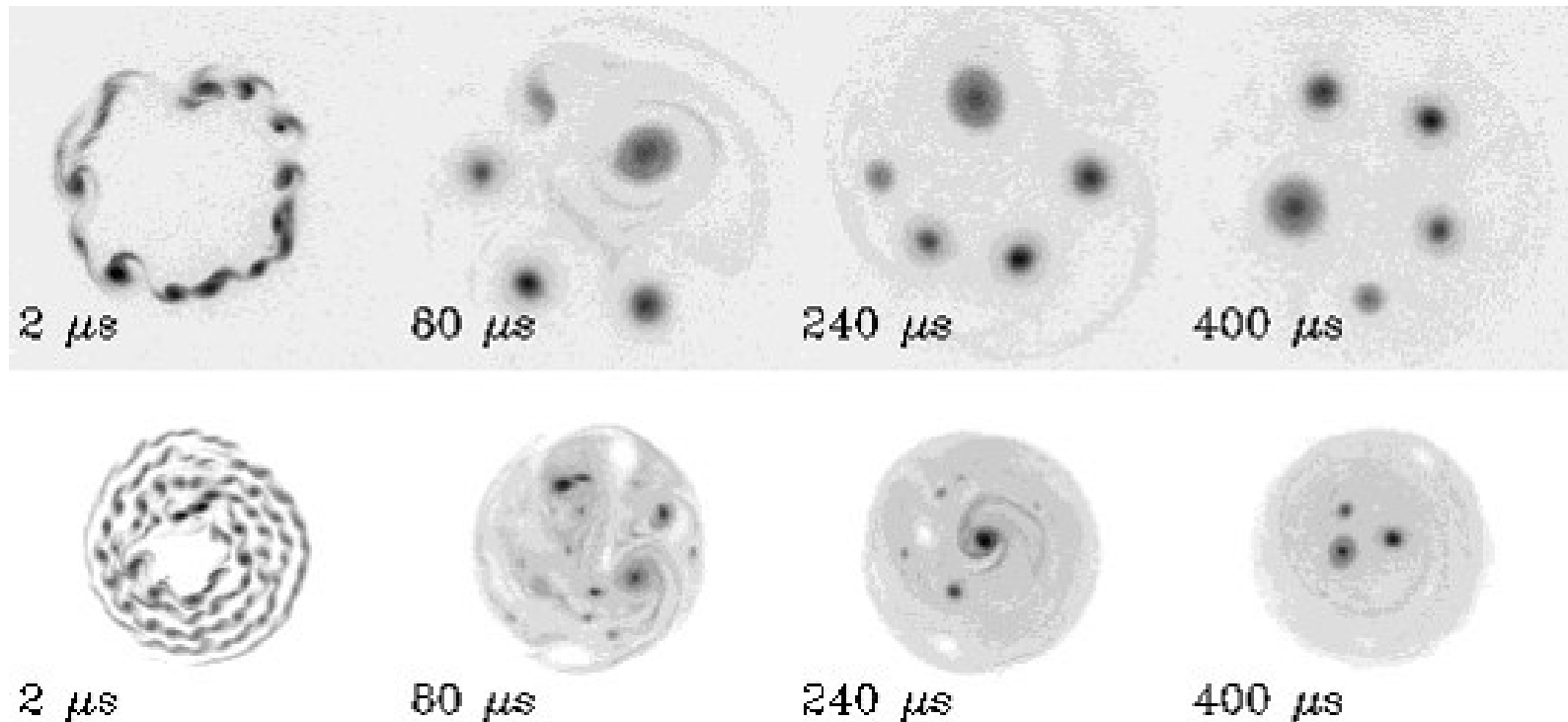
# Annular distributions: evolution [1]

Annular distributions: evolution [2]

The numerical results show in general typical fluid phenomena like the development of the diocotron instability, vortex merging events, the emission of vorticity filaments and the development of a turbulent background.

a) In all cases there is a first stage characterized by the development of the diocotron instability, which leads to the breakup of the annulus into several vortices.

b) After this stage, however, the evolution of plasma changes drastically as r^+ increases, leading to quite different final states. For smaller r^+, the final state consists of a single central patch and a turbulent background, while for larger r^+ final states with multiple vortices can emerge.

Dominant diocotron modes
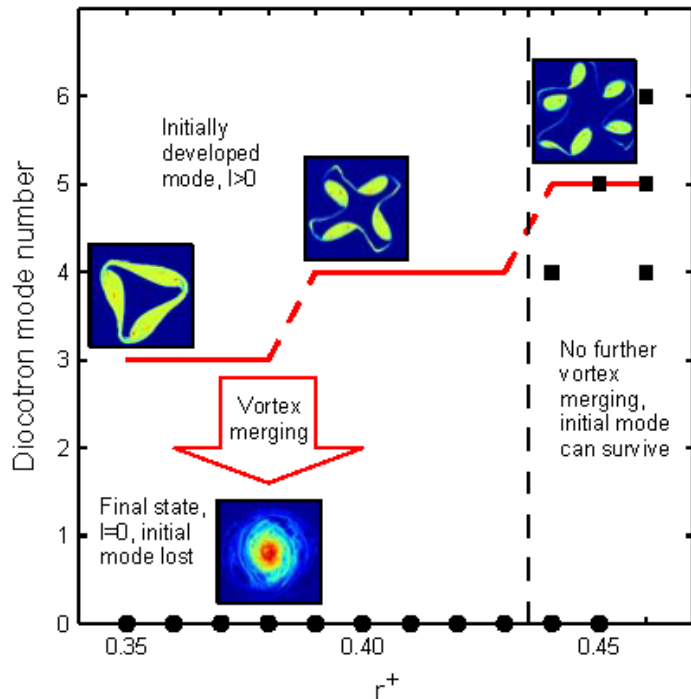
Dominant diocotron mode in the final state versus r^+. The solid circles and squares represent final states with a single central vortex and with multiple vortices, respectively ("$l=0$" indicates axisymmetric states). The red lines indicate the dominant modes as predicted from the linear theory [Davidson, 1990]. Insets show examples of vorticity distributions during the diocotron instability stage.

For low-order dominant diocotron modes, vortex merging processes dominate the plasma evolution up to the formation of a single central vortex, while for higher-order dominant diocotron modes, vortex merging processes can be largely suppressed, and the initially dominant mode leads to the formation of a chain of vortices (vortex crystal), characterized by a number of vortices equal to the order of the same dominant mode.

Influence of fluctuations [1]

In the numerical simulations fluctuations are introduced by the Random Number Generator used to define the initial particle distribution and by the discretization of the system.

A similar situation is found in the experiments, where fluctuations of the initial electron distribution may be due, e.g., to small variations of the source parameters or of the residual gas pressure. For instance, in a sequence of shots using the same plasma trapping time and the same macroscopic injection parameters, the number of surviving strong vortices is not constant.

For small r^+ initial fluctuations have a negligible effect on the plasma evolution, while for large r^+ even very small initial fluctuations can lead to quite different plasma evolutions.

Influence of fluctuations [2]

The non-reproducibility of the final state may be related to the presence of multiple unstable modes with similar growth rates [Chen et al, JPP (2015)].

For small r^+ fewer modes are unstable and the growth rate of the dominant mode is much larger than that of all other modes, so that it will always survive the diocotron instability stage. In these cases ('<u>insensitive</u>'), the effect of initial fluctuations is negligible.

For large r^+ the growth rate of the dominant mode is only slightly greater than that of the second and/or third fastest ones. In these cases ('<u>sensitive</u>'), the development of the diocotron instability depends not only on the growth rate but also on the initial energy of these competing modes.
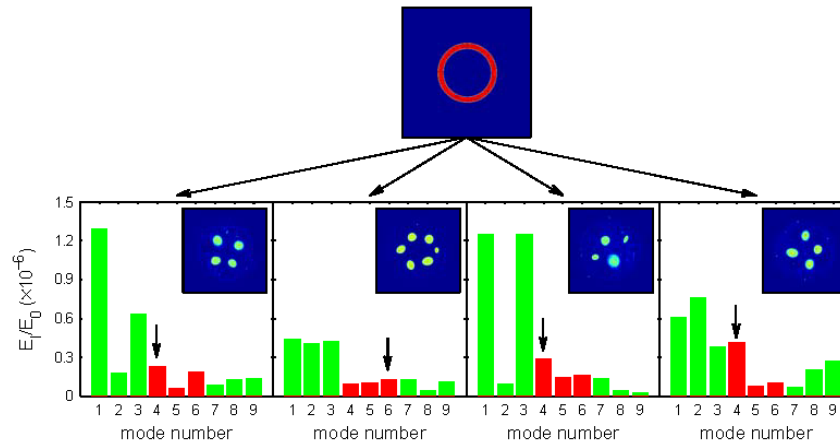
Spiral distributions [1]

Going from an annulus to a spiral with an increasing N_{turns} leads to:
a) formation of a larger number of structures at smaller scales;
b) faster evolution towards a fully developed turbulence.
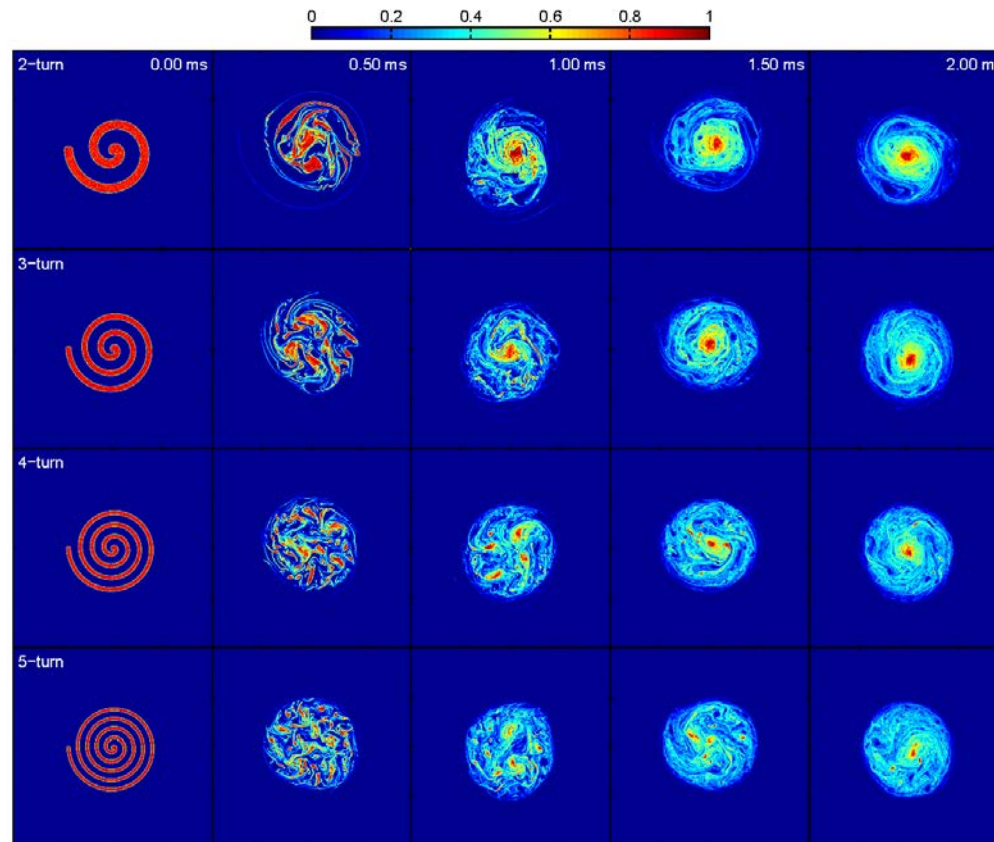
Spiral distributions [2]

The development of the diocotron instability depends strongly on the width of the spiral arms:

a) For thinner spiral arms, diocotron modes with higher mode numbers are more unstable, leading to a larger number of vortices.

b) The spatial scales of the resulting vortices are of the same order as that of the spiral arms, leading to smaller vortices for thinner spiral arms. As N_{turns} increases, the width of the spiral arms decreases and a larger number of small-scale vortices are formed.

These differences in vortex number and spatial scales affect the later evolution of the vorticity distribution. E.g., for N_{turns} = 2, the typical configuration with a central vortex patch and a background forms, while for N_{turns} = 5 small-scale vortices also survive. Such a configuration may be regarded either as a combination of a central vortex/turbulent-background state and a vortex-crystal-like state, or as a modified vortex-crystal-like state with a stronger turbulent background.

Wavelet analysis

One of the characteristic features of the 2D fluid turbulence is <u>intermittency</u>, which is defined as the presence of spatially localized bursts of small scale (high wavenumber) activity of a physical quantity (e.g., vorticity).

Since intermittency is a phenomenon localized in both physical space and spectral space, a suitable analysis tool for its study is the wavelet transform [Farge, ARFM 1992; Mallat, 1999].

A multi-resolution analysis is applied, which successively decomposes the 2D vorticity field into coefficients that contain coarse and fine details at increasing resolution.

Fourier Transform

FT breaks down a signal into constituent sinusoids of different frequencies (transforms the view of the signal from time-base to frequency-base).
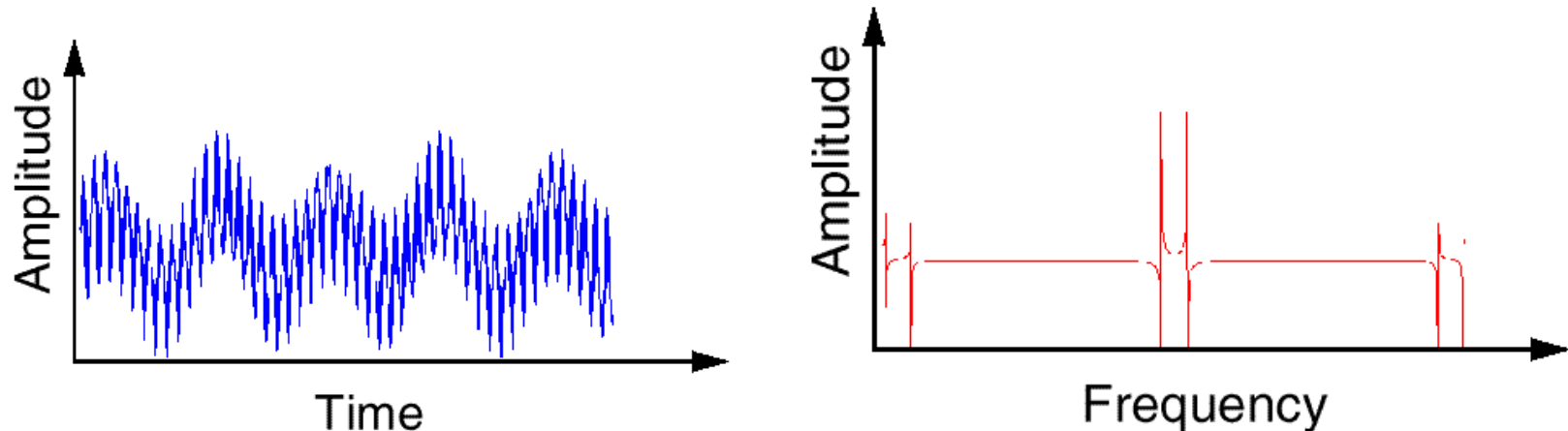
FT provides a signal which is localized only in the frequency domain.
It does not give any information of the signal in the time domain (= "When did a particular event take place?").
FT can not locate drifts, trends, abrupt changes, beginnings and ends of events, etc.
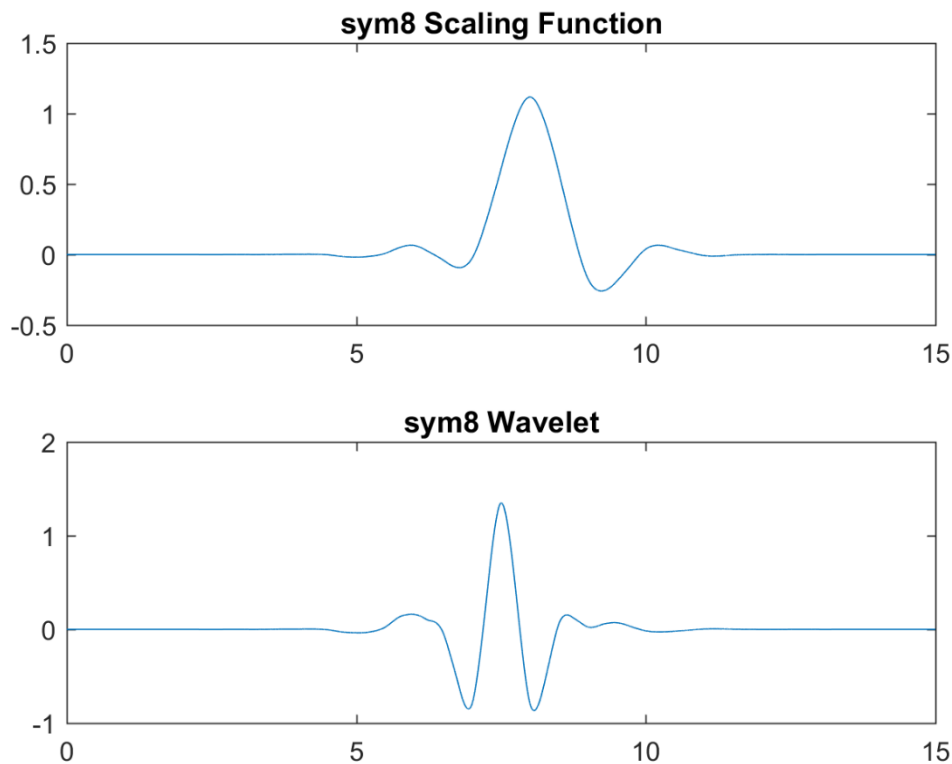
Wavelet Transform [1]

WT: an approach to overcome the resolution problem.

Basis functions of the WT are *small waves* located in different times. They are obtained using scaling and translation of a scaling function and a wavelet function. Therefore, <u>the WT is localized in both time and frequency</u>.

In addition, the WT provides a multiresolution system, i.e., an analysis of the signal at different frequencies with different resolutions (typically: good time resolution and poor frequency resolution at high frequencies; good frequency resolution and poor time resolution at low frequencies).

Wavelet Transform [2]

The mother wavelet is a prototype for generating the other window functions. All the used windows are its dilated or compressed and shifted versions.

sym8 Scaling Function

sym8 Wavelet

$$\psi(s,\tau,t) = \frac{1}{\sqrt{s}} \psi\left(\frac{t-\tau}{s}\right)$$

$$s = 2^{-j}, \ \tau = k \cdot 2^{-j},$$

$$\psi(s,\tau,t) = 2^{j/2} \psi\left(2^{j}t - k\right)$$

$$= \psi_{j,k}(t)$$

Wavelet multi-resolution analysis [1]

In order to separate the <u>coherent and incoherent parts of the flow</u>, an adaptive self-consistent threshold is applied [Farge et al, PoF 1999].
At the i-th step of the iteration, the wavelet coefficients are separated into two classes: those whose modulus is larger than a threshold $\varepsilon_T^{(i)}$, and those whose modulus is smaller. The coherent vorticity field $\zeta_>$ is reconstructed from the strongest wavelet coefficients by an IWT, while the incoherent part $\zeta_<$ is obtained by subtracting the coherent from the total vorticity.

$$\varepsilon_T^{(1)} = [2 < \zeta^2 > \log(N_{grid}^2)]^{1/2}$$

$$< \zeta_<^2 >^{(i)} = (1/N_{grid}^2) \sum \zeta_<^{2(i)}(x,y)$$

$$\varepsilon_T^{(i+1)} = [2 < \zeta_<^2 >^{(i)} \log(N_{grid}^2)]^{1/2}$$
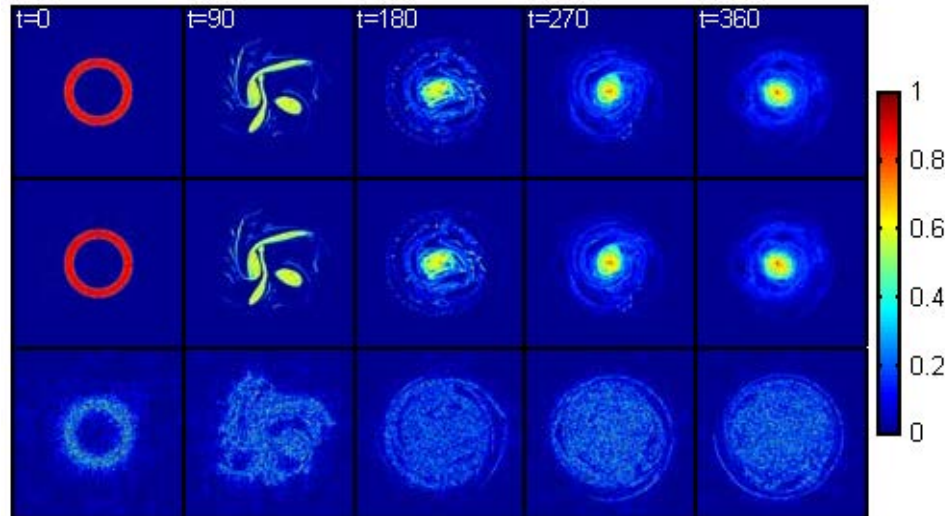
The iteration method is modified in order to take into account the inhomogeneity of the incoherent part, in particular, the fact that the vorticity field is non-zero only in a small fraction of the total domain (i.e. of the grid cells) [Chen et al, JPP 2015].

Wavelet multi-resolution analysis [2]

$r^+/R_w = 0.40$

coherent

incoherent

The data are normalized to their respective maximum values

Only a small fraction (< 2 %) of the wavelet coefficients is necessary to represent the coherent component, which contains the greatest part (> 95 %) of Z_2.
The remaining small-amplitude coefficients represent the incoherent component, and take into account the (numerical) noise and the possible presence of a turbulent background flow.

Enstrophy decay

Enstrophy dissipation occurs mainly during merger events. Filaments of vorticity are stripped off the vortices and continue to elongate until their transverse spatial scale becomes smaller than a characteristic scale length (cell width for the PIC simulations, Larmor radius in the real system), at which the enstrophy they contain is dissipated.
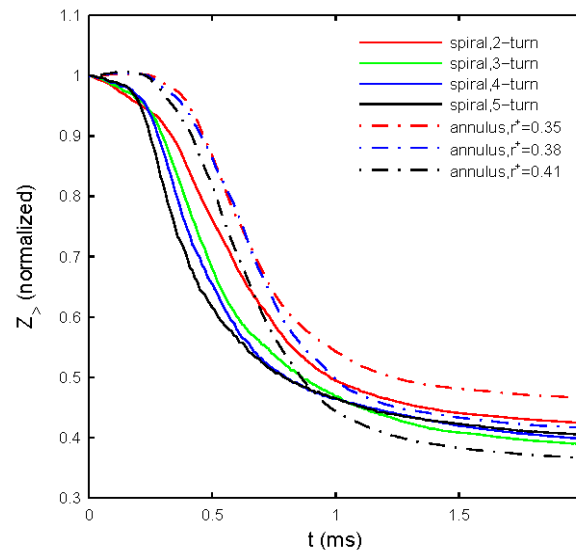
During the vortex merger stage, the coherent part of the enstrophy is more rapidly dissipated and transferred to the turbulent background as N_{turns} increases. A similar phenomenon is observed for annular initial distributions (Note: the widths of the spiral arms are always smaller than the widths of the considered annular configurations).

Coherent enstrophy spectra

The maximum wavenumber k_{max} of the spectrum is the inverse of the minimum spatial scale of the wavelet functions (which is twice the length of a grid cell), i.e. $k_{max} = 1/[2*(2/N_{grid})]$ (the wavenumber is normalized over $1/R_w$). In each successive decomposition level the spatial scale of the wavelet functions is increased by a factor of 2 and k is accordingly divided by 2, up to a maximum level of ($\log_2 N_{grid} - 1$), i.e. up to a minimum wavenumber $k_{min} = 1$.
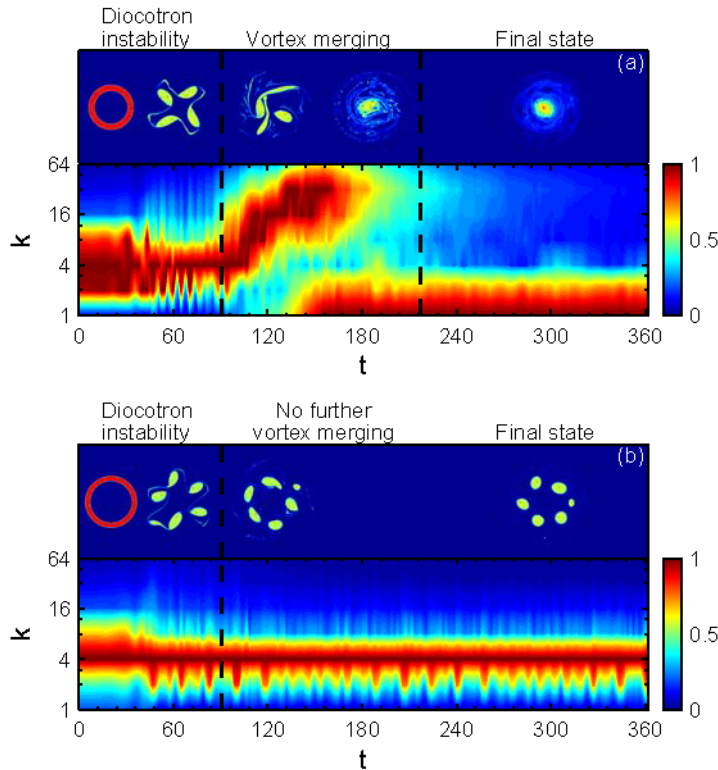
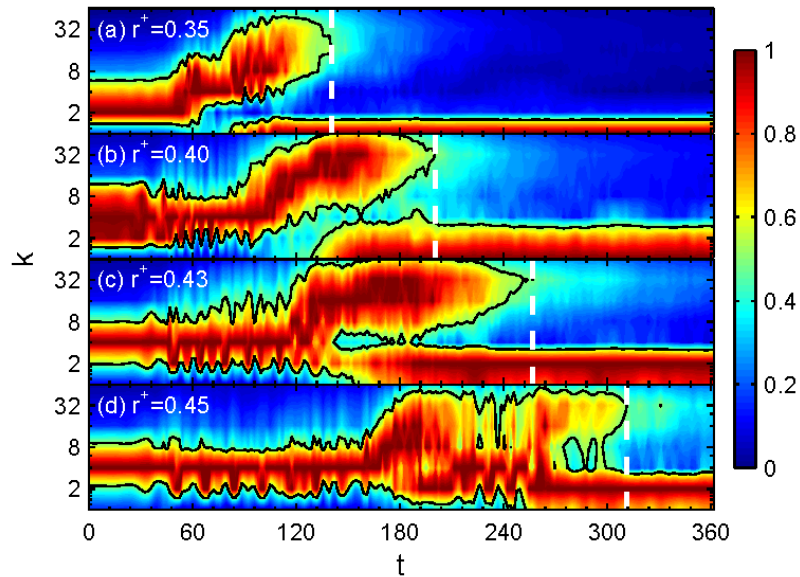Coherent Z_2-spectrum (normalized by its maximum value) for
(a) r^+/R_w = 0.40:
(b) r^+/R_w = 0.46.

The vortex merging stage is related to the time interval in which the spectrum shows a "bifurcation" structure.

Chen et al, JPP 2015

Time of turbulence development [1]

1) During the diocotron instability stage, the annulus breaks into several vortices, whose spatial scale is roughly the same as that of the annulus. The peak of the enstrophy spectrum (red region) remains close to its initial position.

2) During the merging process the vortices become highly deformed, and emit vortex filaments. Enstrophy is transferred into components of both larger (central vortex) and smaller (vortex filaments) spatial scales (bifurcation of the spectrum).

3) At the end of the merging stage, vortex filaments evolve into a turbulent background, losing their identity. The branch at smaller spatial scales in the spectrum disappears.

The instant at which the branch at larger k falls below a given value (e.g., half of the maximum value), is regarded as the <u>time of turbulence development</u>, T_{turb}.

Time of turbulence development [2]
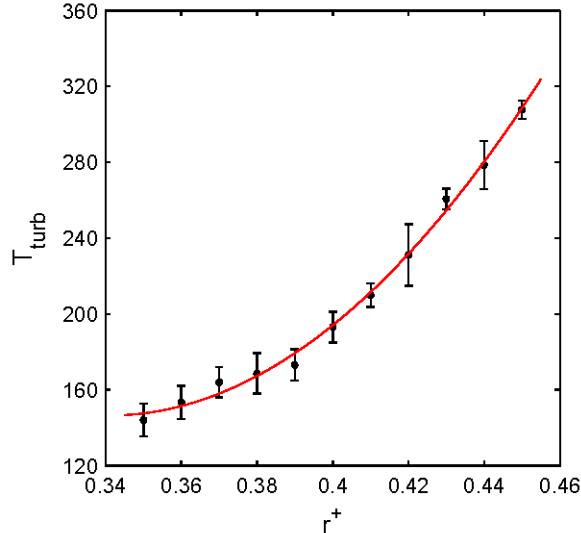
Several simulations are carried out for each r^+, so that the average of the values of T_{turb} is shown, together with an error bar corresponding to one standard deviation. The data are compatible with a quadratic dependence with r^+.

General mechanism: the vortex filaments become thinner and thinner with time and the strong vortices tend to move towards the center, while the canonical angular momentum of the system is kept constant during the evolution.

As r^+ increases, the effective area that can be covered by the turbulent background the time needed to obtain an almost uniform background also increase.

In addition, as the dominant mode shifts to higher mode numbers, more vortices are generated before the vortex merging stage actually begins. The typical size of these vortices becomes smaller, while the average distance between the vortices gets larger, so that it takes more time for vortex merging to complete, and the evolution of turbulence is slowed down.

# Spiral distributions: Coherent enstrophy spectra
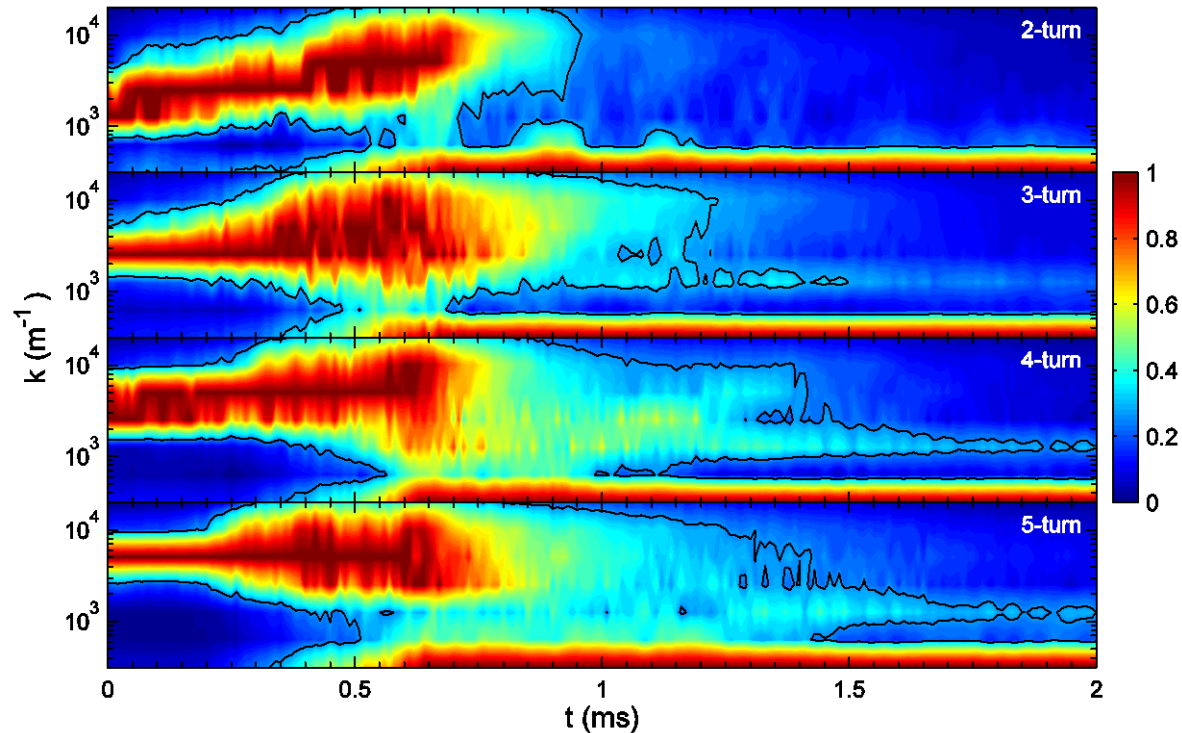
For spiral distributions, as N_{turns} increases the coherent Z_2-spectrum shows that the vortex structures (formed at increasingly smaller scales) become more persistent, and it is again possible to estimate the time required to reach a state of fully developed turbulence.

Romé et al, PSST 2016

Other statistical investigations

Using the results of the numerical simulations, the scaling properties of electron density are analyzed by computing their PDFs and structure functions.

In turbulence studies the analysis of the <u>scaling properties of the field increment statistics</u> provides information about the presence of coherent structures, such as vortices or shocks, and about their typical spatial scales [Frisch, 1995].

u(x)

u(x+r)

$$\Delta u(r) = u(x+r) - u(x)$$
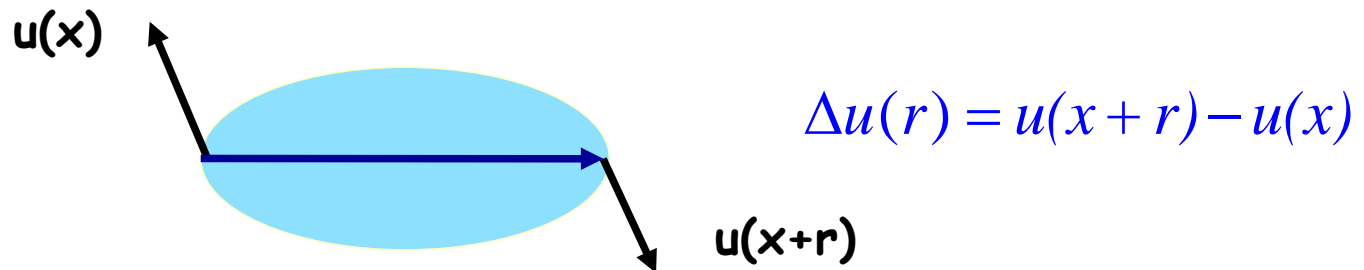
Probability distribution functions and flatness

The scaling behavior of the vorticity increments in both *x* and *y* directions are considered:

$$\Delta\zeta_l^{(x)}(x,y,t) = \zeta(x+l,y,t) - \zeta(x,y,t);$$

$$\Delta\zeta_l^{(y)}(x,y,t) = \zeta(x,y+l,t) - \zeta(x,y,t).$$

One of the basic signatures of intermittency is the change in the PDF shape with the scale *l*. In order to compare the shape of the PDFs at different scales in an effective way, normalized increments are used, defined as

$$\Delta\zeta_{l,st} = \frac{\Delta\zeta_l - <\Delta\zeta_l>}{\sigma_{\Delta\zeta_l}};$$

More quantitative information about the scaling properties of field increments is obtained from the analysis of the so-called structure functions, defined as the moments of field increments, $S_p(l) = \langle\Delta\zeta_l^p\rangle$, where $\langle\cdot\rangle$ denotes spatial averages. Intermittency is typically quantified by means of the flatness, defined as $F(l) = S_4(l)/[S_2(l)]2$ (= 3 for a Gaussian PDF).

Example of PDF evolution
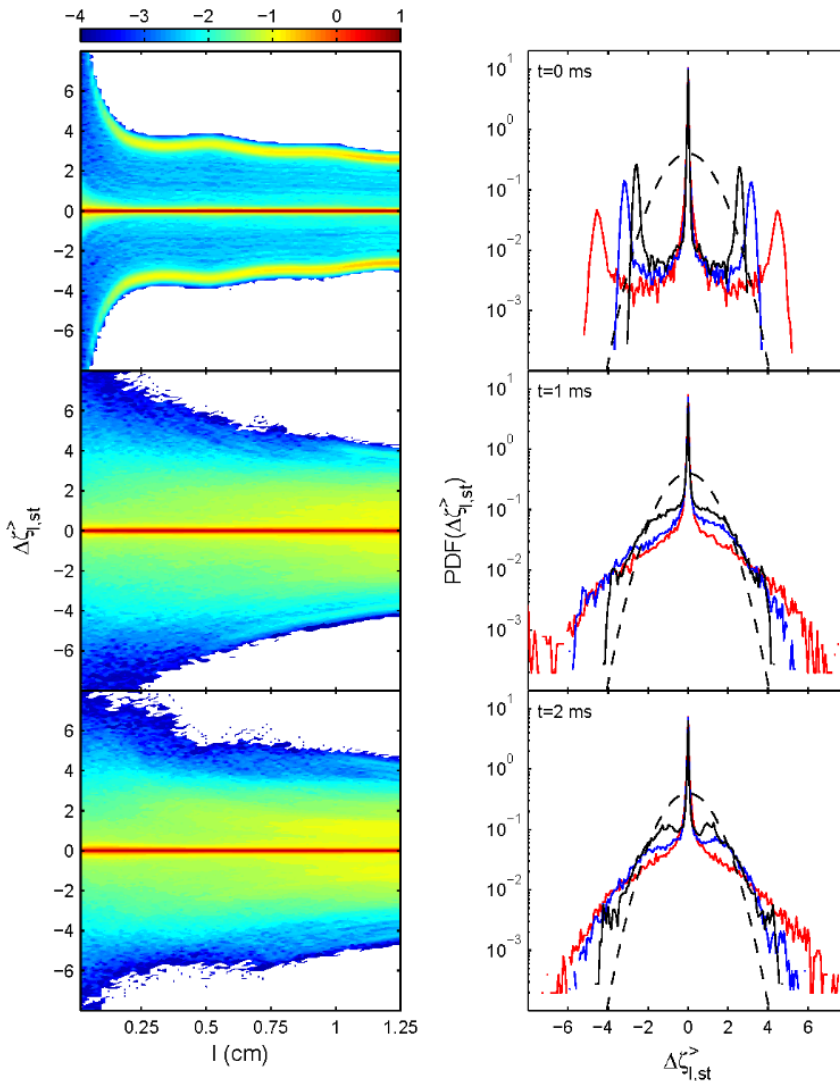
PDFs of the normalized vorticity increments for the coherent part of the flow for N_{turns} = 2. PDFs for l = 0.125 cm (red), 0.625 cm (blue) and 1.25 cm (black). Also shown is the normalized Gaussian distribution (black dashed line), with zero mean and unitary standard deviation.

At t=0, the PDFs are different from Gaussians due to the regularity (non-turbulent nature) of the initial conditions. As turbulence develops, the PDFs evolve towards, but still remain different from, a Gaussian distribution. At later times, two bumps appear at both sides of the central peak which are related to the well-developed turbulent background, that contributes approximately as a Gaussian distribution with a non-zero average (due to the single sign of the vorticity field).

Example of flatness evolution
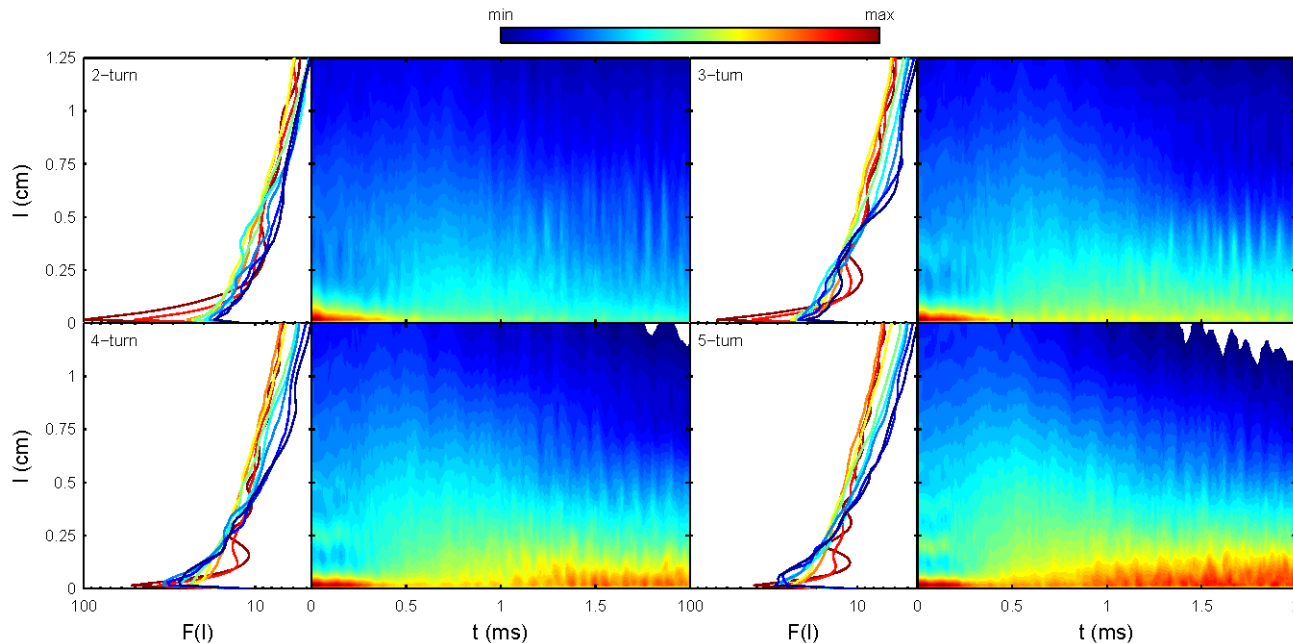
t = 0 (dark red), 0.25 (red), 0.5 (orange), 0.75 (yellow), 1.0 (light green), 1.25 (green), 1.5 (light blue), 1.75 (blue), and 2.0 ms (dark purple).

a) Due to the step-like distribution of the initial vorticity, F(l) grows as l decreases, with a series of sharp peaks down to l = 0.02 cm. Such growth of F(l) does not correspond to a real intermittency.

b) In fact, these initial peaks shrink to much lower values during the diocotron instability development (processes such as instability growth, vortex formation, and filament emission tend to smooth the initial step function).

c) Later, however, the growth of F(l) at small l becomes stronger and stronger, as N_{turns} increases, indicating strong intermittency.

Forced dynamics

Introduction

Study of the role that non-axisymmetric, multipolar radio frequency (RF) drives applied to the cylindrical (circular) boundary play on the insurgence of azimuthal instabilities and the subsequent formation of coherent structures preventing the relaxation to a fully developed turbulent state (the frequencies and the spatial structure of the applied electric drives considered in the simulations are experimentally relevant).

The aim is to understand how energy is injected into the system by an external non-axisymmetric forcing, in terms of the spatial scales and the plasma modes involved, and the localization of energy and enstrophy structures.
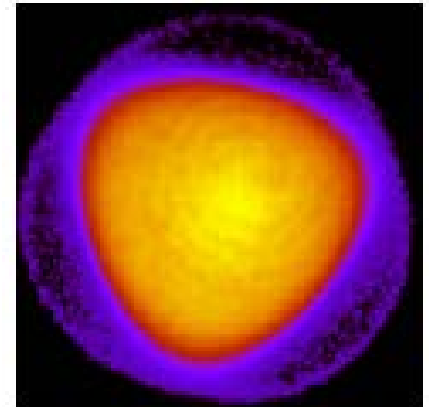
External forcing

$$\phi_w^{co,ctr}(\theta,t) = \sum_{m=0}^{3} V_{RF} \cos(2\pi v_{RF} t + \sigma m \pi / 2) \times$$
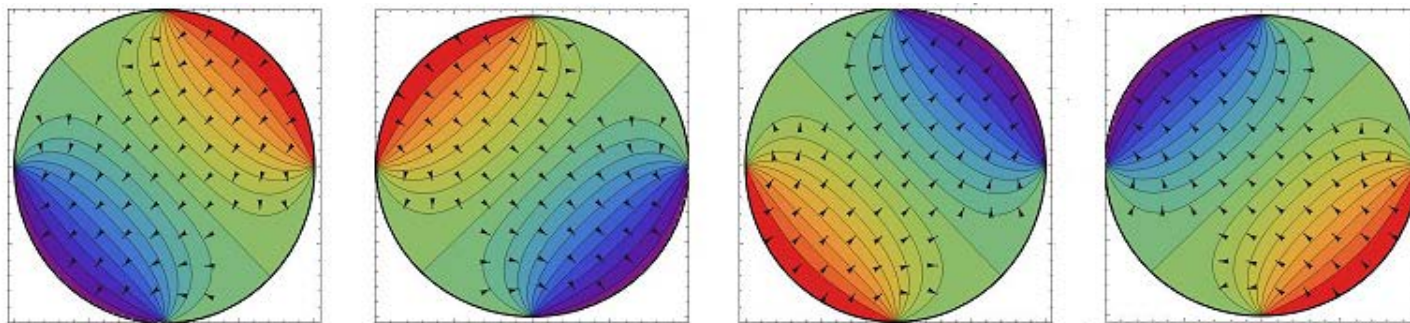$$[H(\theta - m\pi / 2) - H(\theta - (m+1)\pi / 2)]$$
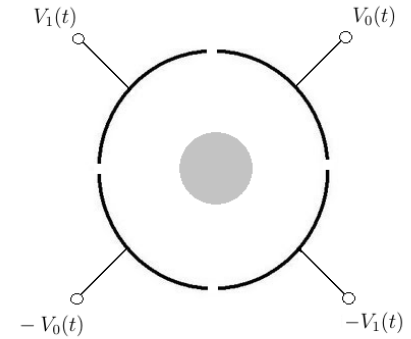
σ = -1 and σ = -1 correspond to 'co-' and 'counter-rotating' drives with respect to the electron plasma azimuthal motion, respectively.

Rotating electric fields give rise to non-trivial mode amplification (e.g. the l = 3 mode in a counter-rotating configuration [Bettega et al, JAP2009]).
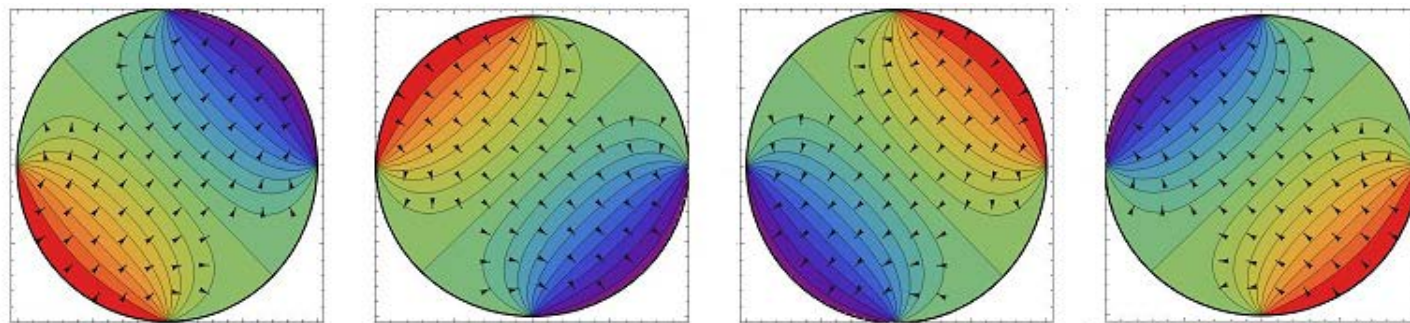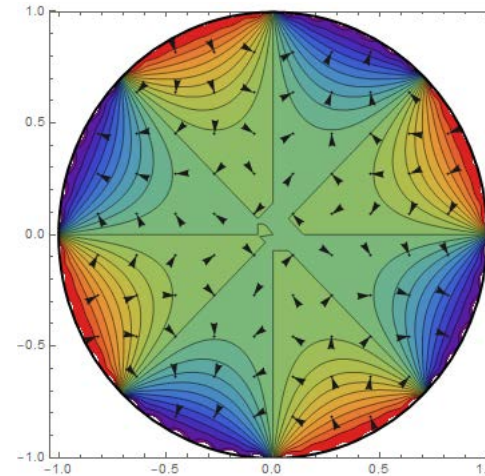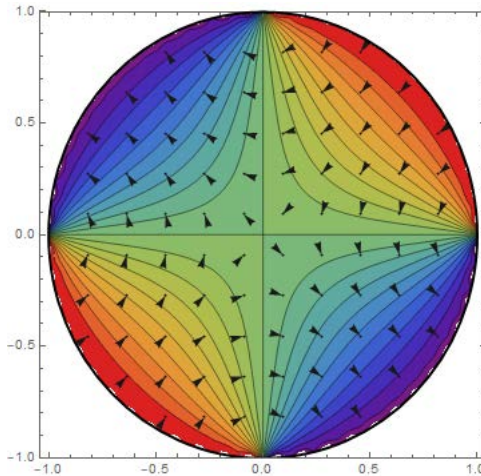
Rotating dipole drives

σ=1

σ=-1

Multipolar drives (non-rotating)

$$\phi_w^{quad}(\theta,t) = V_{RF}\cos(2\pi\nu_{RF}t)\sum_{m=0}^{3}(-1)^m H(\theta - m\pi/2)$$

$$\phi_w^{octu}(\theta,t) = V_{RF}\cos(2\pi\nu_{RF}t)\sum_{m=0}^{7}(-1)^m H(\theta - m\pi/4)$$

First set of simulations: parameters

Reference annular distribution; r^-/R_w = 0.36, r^+/R_w = 0.45.

Co- and counter-rotating dipole and oscillating quadrupole drives.

V_{RF} = 0.10 V (the maximum of the plasma potential $|Vp|$ is 2.2 V, evaluated for the reference annular density profile in the case of a grounded cylindrical wall).

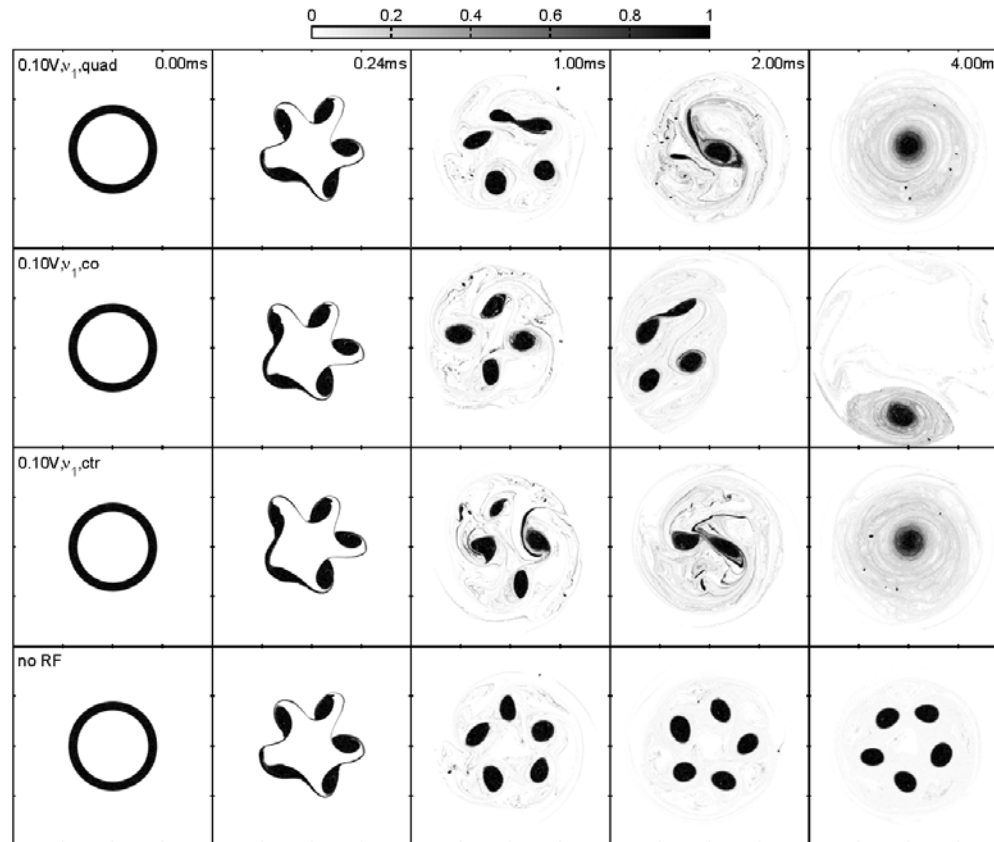v_{RF} = 1.05 kHz ≈ v_1, 7.82 kHz ≈ v_3, 12.92 kHz ≈ v_5 (range of frequencies where the dynamical evolution of the lowest order azimuthal modes is expected to be significantly affected).

N_{grid} = 256.

N_{macro} = $1.0 \cdot 10^6$.

t_f = 4 ms.

Electron density evolution for different RF drives (v_{RF} = 1.05 kHz).

Annular distributions: vorticity evolution [2]

a) In the case of the quadrupole drive, the shape and position of both vortex patches and filaments are almost unchanged during the diocotron instability stage with respect to the no-RF case, indicating a negligible effect of the quadrupole drive during this time interval. However, vortex merger events occur later resulting in a collapsed state, which is maintained until the end of the simulation, with one central vortex patch and a much stronger turbulent background than for the no-RF case.

b) The co- and counter-rotating drives show stronger effects on plasma evolution. Slight changes of the vortex filaments are already visible during the diocotron instability stage. After that, vortex merger processes also occur, leading to a fully collapsed final state. The change of the evolution is particularly dramatic for the co-rotating case, even if V_{RF} is relatively small. A strong l = 1 mode is resonantly driven in this case, the plasma is pushed off-axis and a non-negligible fraction (10%) of the particles is lost at the wall.
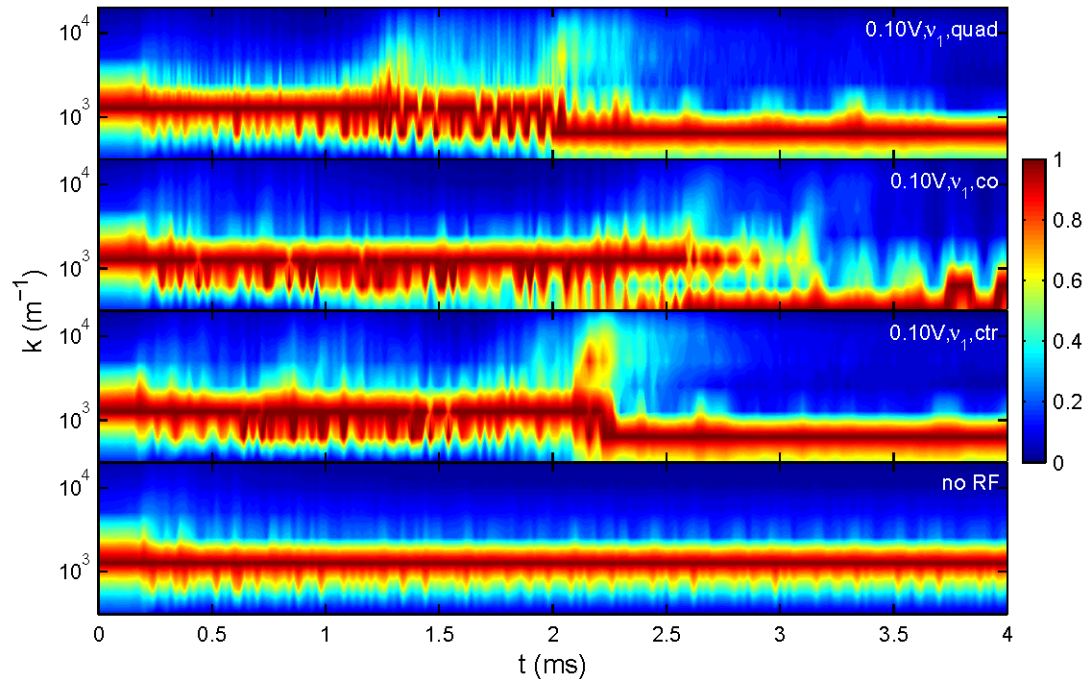
Enstrophy evolution
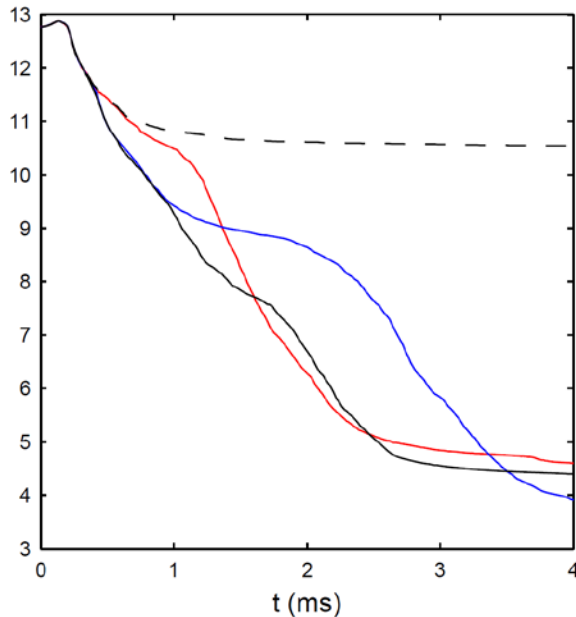
Enstrophy evolution for quadrupole (red), co- (blue), counter-rotating (black) drives, and no-RF case (black dashed curves).

a) The (coherent part) of the enstrophy remains larger for the no-RF case, due to the surviving vortex crystal-like final state and the weakest turbulent background.
b) The quadrupole and counter-rotating cases show similar trends, since both undergo a series of vortex merger processes and end up with a fully collapsed state.
c) For the co-rotating drive, the rapid decreases correspond to vortex merger processes, while the slow decrease corresponds to a time interval of almost rigid rotation between major vortex mergers. The enstrophy falls below the values reached in the other cases, due to the excited $l = 1$ mode and the consequent particle loss.

Enstrophy spectrum evolution

Comparison of the coherent enstrophy spectrum evolution for quadrupole (first row), co- (second row) and counter-rotating (third row) drives. The last row corresponds to the no-RF case.

Romé et al, PPCF 2017

Second set of simulations: parameters

Reference annular distribution; r^-/R_w = 03724, r^+/R_w = 0.46.

Quadrupolar and octupolar drives.

V_{RF} = 0.50 V (the maximum of the plasma potential $|Vp|$ is 2.31 V, evaluated for the reference annular density profile in the case of a grounded cylindrical wall).

v_{RF} = 1.05 kHz ≈ v_1 or v_{RF} = 5.145 kHz ≈ v_2.

N_{grid} = 512.

N_{macro} = 2.5 · 10^6.

t_f = 4 ms.
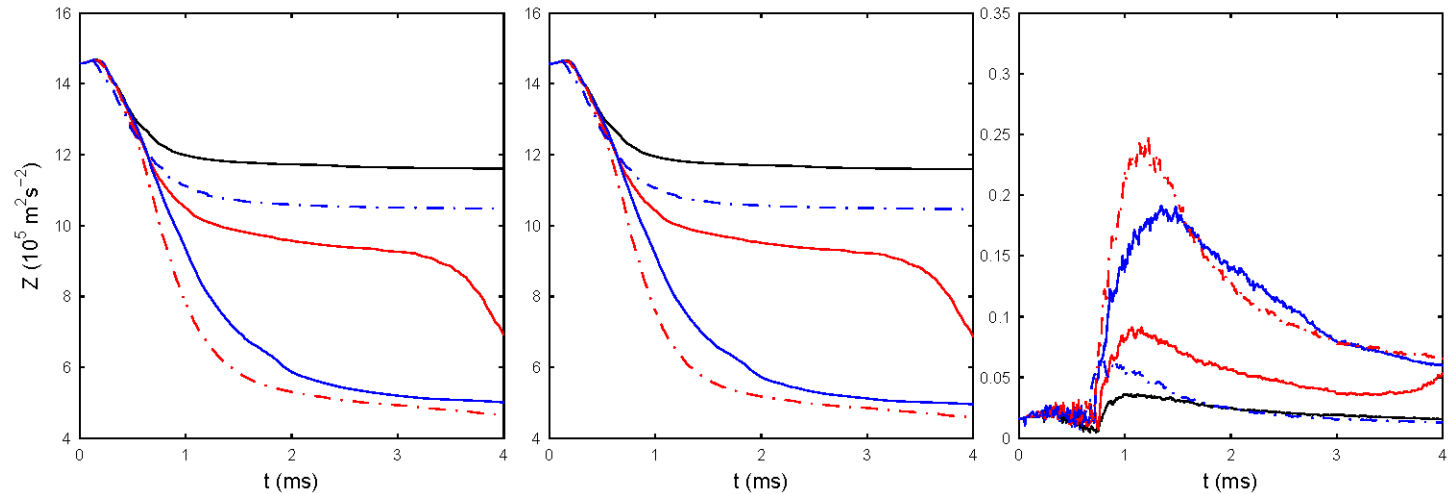
Annular distributions: vorticity evolution [1]
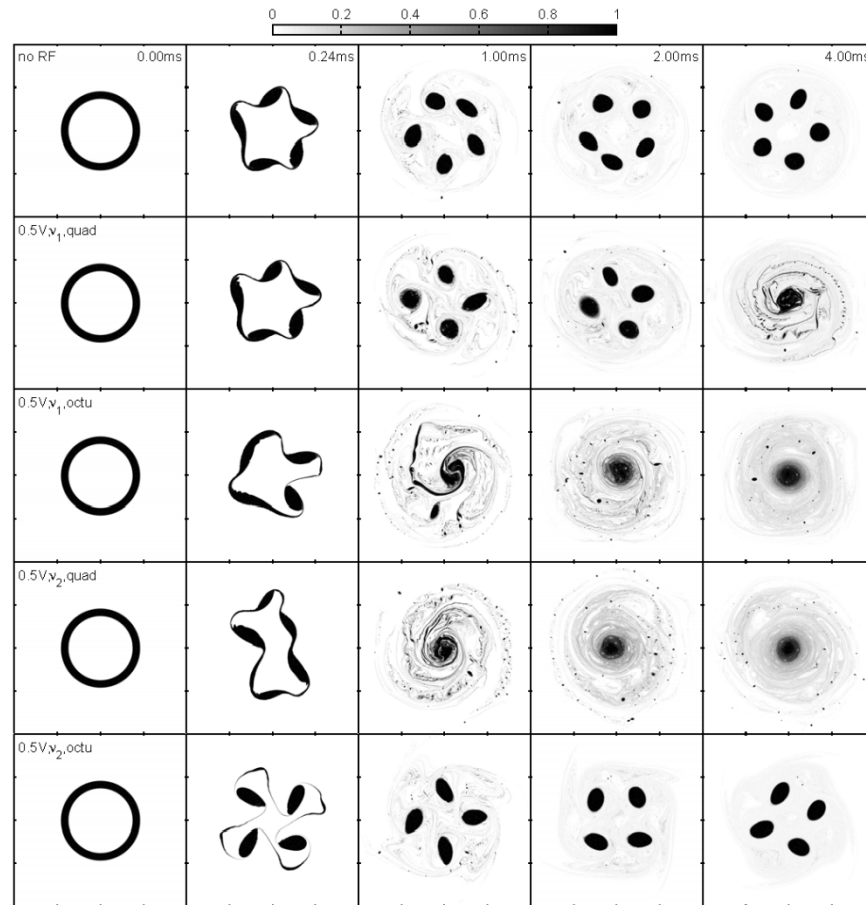
(a) No external drive is present; (b,c) v_{RF} = 1.05 kHz, (d,e) v_{RF} = 5.145 kHz.

Chen et al, JPP 2017

Annular distributions: vorticity evolution [2]

a) In the case of a quadrupole drive with $v_{RF} \approx v_1$, the shape and position of both vortex patches and filaments show only slight changes during the diocotron instability stage with respect to the no RF case.

b) However, when $v_{RF} \approx v_2$, five highly distorted vortex patches with an elongated configuration are formed. This elongation of the vortex configuration is indicative of the influence of a strong $l = 2$ mode, in accordance with the azimuthal symmetry of the quadrupole drive.

c) Likewise, the octupole drive seems to stimulate a competing or even overwhelming $l = 4$ mode. In the case of an octupole drive with a frequency close to v_1, a considerable development of the $l = 4$ mode occurs together with the evolution of the most unstable $l = 5$ mode.

d) For a drive frequency close to v_2, the $l = 4$ mode becomes the fastest-growing mode, forming a quite symmetric four-vortex patch configuration.

e) This effect of the azimuthal symmetry of the drive remains evident until the end of simulation. In particular, the turbulent backgrounds show elliptical and square shapes for the quadrupole and octupole drives, respectively.

Annular distributions: enstrophy evolution

Comparison of the total (a), coherent (b) and incoherent (c) enstrophy evolution for a drive at v_{RF} = 1.05 kHz (quadrupole, red solid), (octupole, blue solid), and at v_{RF} = 5.145 kHz (quadrupole, red dash-dotted) (octupole, blue dash-dotted). The corresponding enstrophy evolutions for the no RF case (black solid curves) are also plotted.

Annular distributions: enstrophy spectrum evolution
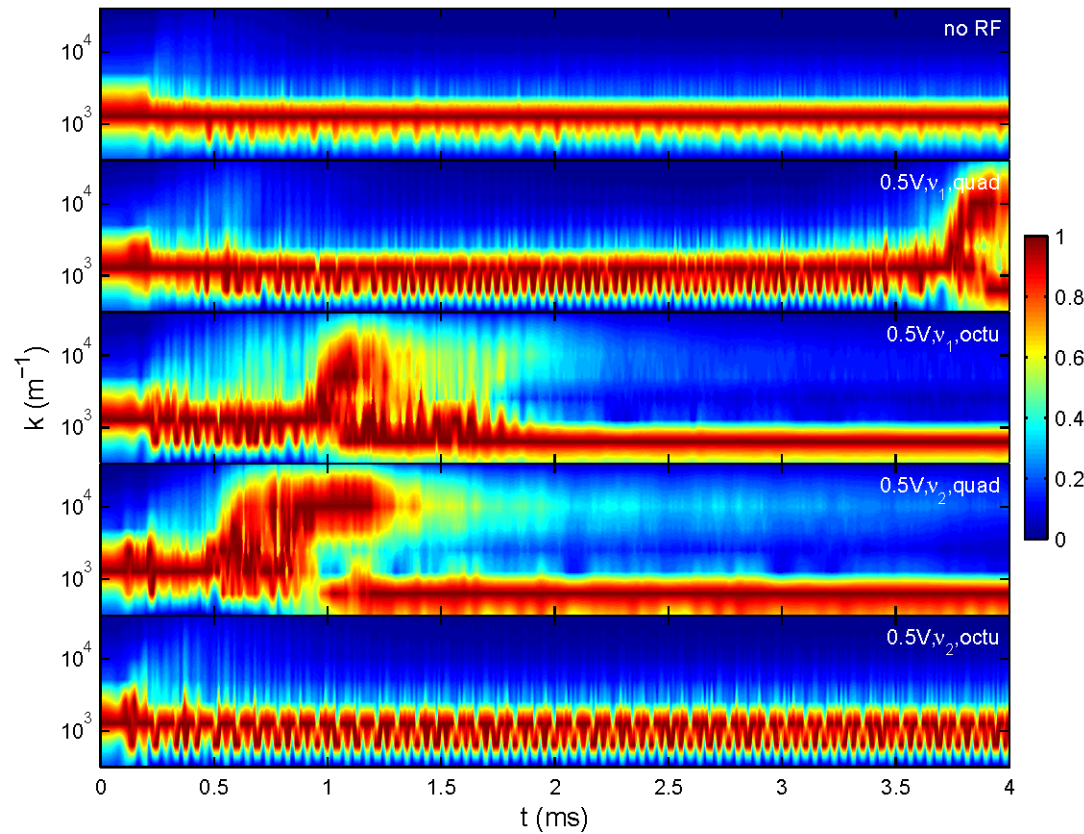
Chen et al, JPP 2017

Chen et al, JPP 2017

Spiral distributions: vorticity evolution [2]

a) The quadrupole drives have an observable effect during the diocotron instability stage, especially for the higher frequency v_2. The elongation of the vortex configuration is clear at the end of diocotron instability stage, and the turbulent background also shows an elliptical shape.
b) On the other hand, the octupole drives have negligible effect during the diocotron instability stage, resulting in a very similar distribution for both the vortex patches and the filaments. The effect of the drive is more evident during the later stage, leading to a square-shaped turbulent background at the end of the simulations.

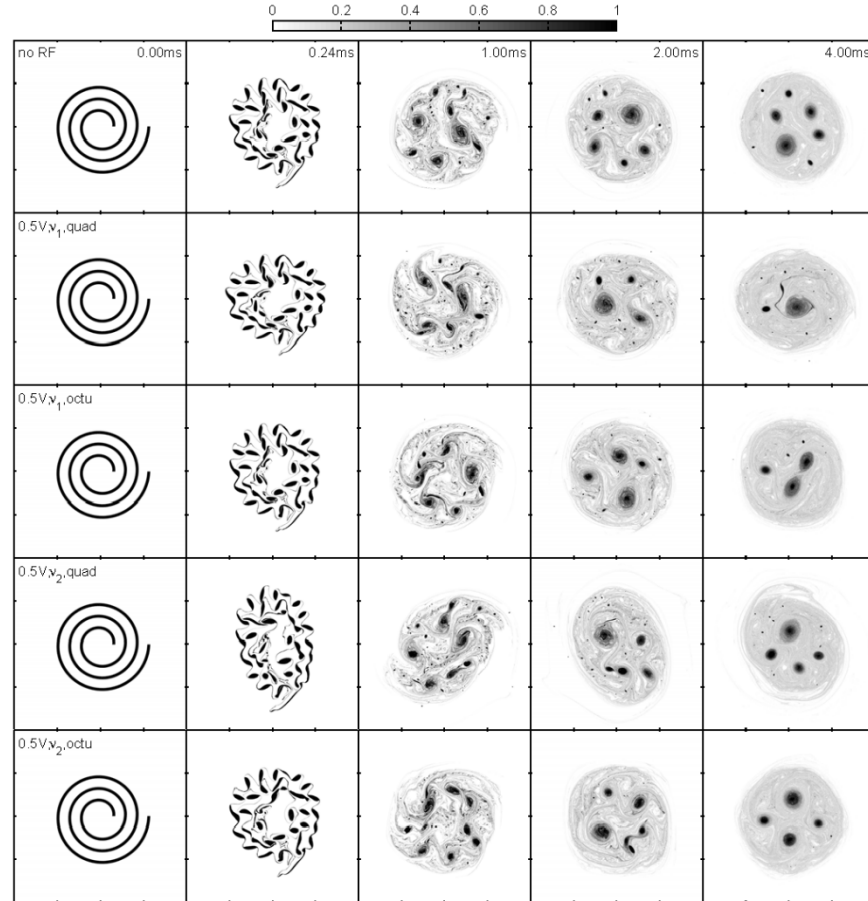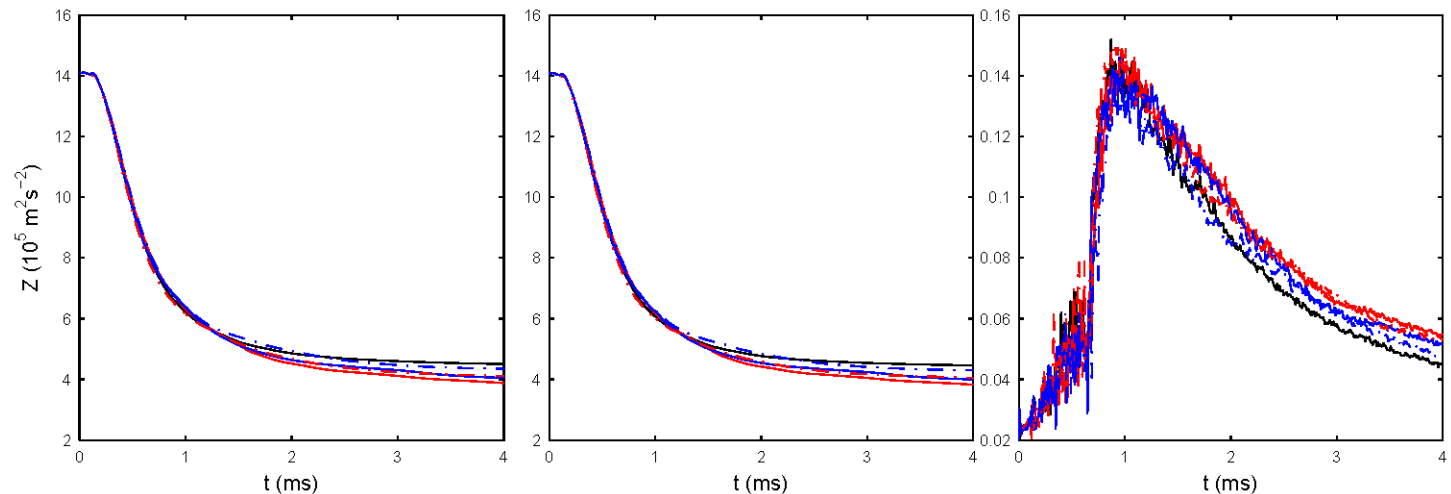Apart from some details, all cases show a similar trend for the plasma evolution.

Comparison of the total (a), coherent (b) and incoherent (c) enstrophy evolution for a drive at v_{RF} = 1.05 kHz (quadrupole, red solid), (octupole, blue solid), and at v_{RF} = 5.145 kHz (quadrupole, red dash-dotted) (octupole, blue dash-dotted). The corresponding enstrophy evolutions for the no RF case (black solid curves) are also plotted.

Chen et al, JPP 2017

Results [1]

In the case of annular initial configurations, the dynamics is in general characterized by a low level of turbulence and is punctuated by time limited or indefinite persistence of coherent vortices. These features are marked in the enstrophy evolution by stages of stasis and abrupt changes or bifurcations in the spatial scales corresponding to maximum enstrophy content. The effect of the azimuthal symmetry of the drive remains evident until the end of simulation (for instance, the turbulent backgrounds show elliptical and square shapes for the quadrupole and octupole drives, respectively).

On the contrary, in the case of spiral-like initial distributions the dynamics is inherently more complicated and characterized by a stronger intermittency, with multiple vortices and frequent merger events during the evolution. Despite some small differences in the time evolution caused by the different external forces, the intermittency levels for the considered regime of forcings and the range of frequencies corresponding to the low-order diocotron modes are approximately the same.

Results [2]

The analysis of several runs for each set of drive amplitude, frequency and multipolar drive shows that different final states (e.g. number of vortices) can be reached irrespective of the type of drive. The effect of the drives is therefore mediated by the strong influence of the fluctuation of the initial conditions, which, as already shown in the case of free-decaying turbulence dramatically affects the evolution towards multiple-vortex intermediate or final states.

Conclusions and perspectives

General conclusions [1]

In general, the evolution of the 2D turbulence is essentially controlled by the dynamics and interactions of the vortices, which depend on their size, separation, intensity and on the background shear. The emergence of the vortices is due to the nonlinear development of the diocotron instability, that strongly depends on the initial density distribution and on the influence of a possible external forcing.

Both for the free relaxation and in the presence of a (weak) external forcing, the fluctuations, e.g. inhomogeneities in the initial density (vorticity) distributions play a dramatic role in determining whether a single patch equilibrium state can be reached or the relaxation is temporarily or indefinitely halted by the occurrence of intermittent phenomena such as localized vortices.

General conclusions [2]

Thanks to their localization both in physical and wavenumber space, wavelets allow for better discrimination with respect to the Fourier analysis of evolving coherent structures with different spatial scales in the flow, and therefore for a more accurate and detailed description of intermittency phenomena.

The wavelet analysis allows one to clearly relate the presence of time periods characterized by a decreasing coherent enstrophy and the existence of bifurcation structures in the relevant spectra (with the transfer of enstrophy to both large and small spatial scales) to the occurrence of (possibly repeated and time-separated) vortex merger processes in the flow. A relation between the initial conditions and the time required to achieve a state of fully developed turbulence has been shown.

General conclusions [3]

In general, a larger enstrophy dissipation is detected in the presence of an external RF drive due to the additional differential velocity field (shear) induced by the injection of enstrophy and energy at the scale of the forcing (and depending on the forcing).

In previous studies of the free relaxation of the 2D turbulence of an electron plasma, the dynamics of the system was characterized by a monotonically decreasing enstrophy evolution, for which a similarity decay law was proposed [Rodgers et al, PRL 2010].
The numerical simulations show that in the case of free relaxation different initial distributions lead to different times for the development of turbulence. In the presence of external forcing, stages are detected where vortex mergers are interrupted by the formation of metastable states which evolve in a rigidly rotating way.

Can these results be applied or suggest something on the turbulence evolution in other fluid systems?

Perspectives: Numerical investigations

More insight on the turbulent evolution of an electron plasma may come from the study of:

- the <u>role of the turbulent background</u> (e.g., evaluating the effect of random background distributions of varying intensity superimposed on an assigned electron density, possibly with a smooth profile as opposed to the step-like ones simulated so far);

- the influence of the distribution and concentration of a <u>second population of charged particles</u> [Sengupta et al, PoP 2015, PoP 2016, PoP2017; Saitoh et al, NJP2015; Himura, NIMA 2016];

- the effect of higher-frequency and/or higher-amplitude drives;

- the effect of <u>dissipation</u> (e.g., resistive loads on the circular conducting trap wall).

Perspectives: Experimental investigations
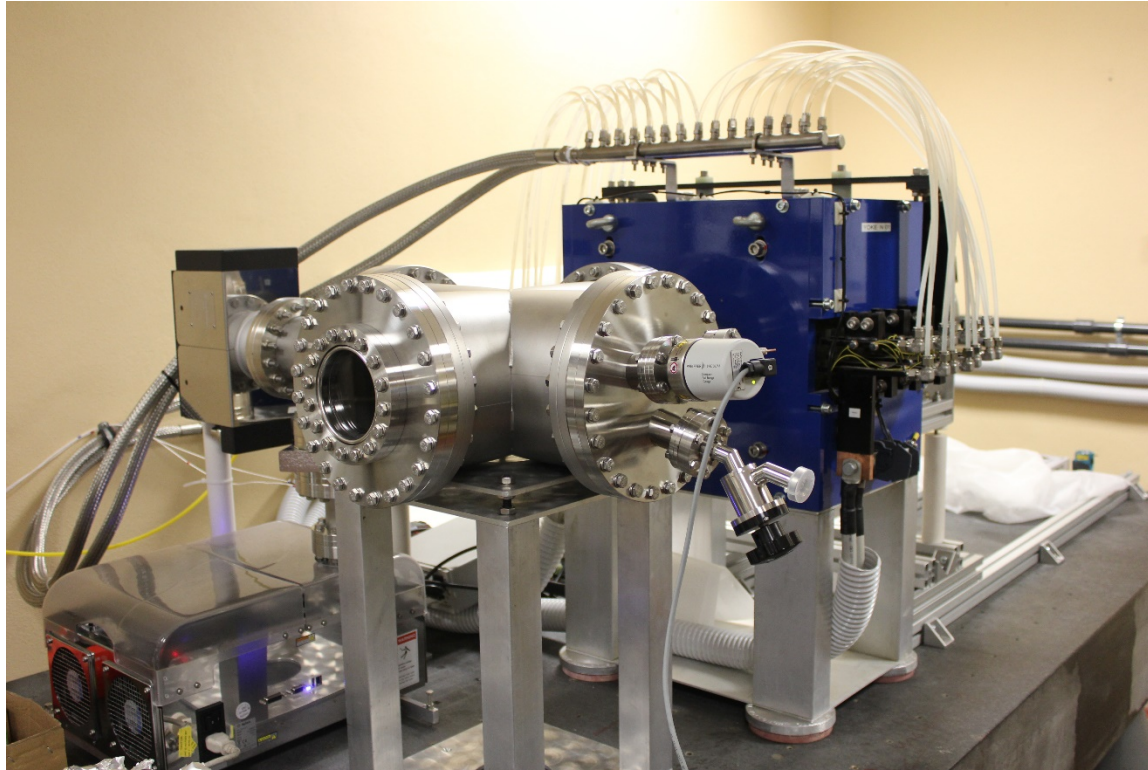
The DuEl set-up offers the chance to study the dynamics of a <u>non-neutral complex plasma</u>, and in particular the influence of a charged dust population on the turbulence evolution of an electron plasma.

Thank you!

Thank you for your attention!

website: http://plasma.fisica.unimi.it